New Heterocyclic Adenosine Receptor Ligands through Molecular Simplification Strategies

Letizia Crocetti[a1*], Abigail Pearce[b1], Venkat S. Vege[b1], Qi Xu[c1], Jing Xu[c], Hannes Buthmann[b], Maria Paola Giovannoni[a], Gabriella Guerrini[a], Francesca Catarzi[a], Silvia Selleri[a], Xianglin Huang[b], Aneesh Chandran[b,d], Graham Ladds[b**], Agostino Cilibrizzi[c***]

[a]*NEUROFARBA, Pharmaceutical and Nutraceutical Section, University of Florence, Via Ugo Schiff 6, 50019 Sesto Fiorentino, Italy*

[b]*Department of Pharmacology, University of Cambridge, Tennis Court Road, Cambridge, CB2 1PD, UK*

[c]*Institute of Pharmaceutical Science, King's College London, Stamford Street, London SE1 9NH, UK*

[d]*Department of Biotechnology & Microbiology, Kannur University, Kannur 670 661, Kerala, India*

***Corresponding author:** Letizia Crocetti, email: letizia.crocetti@unifi.it

****Corresponding author:** Graham Ladds, email: grl30@cam.ac.uk

*****Corresponding author:** Agostino Cilibrizzi, email: agostino.cilibrizzi@kcl.ac.uk

[1] These four authors contributed equally to this article.

Abstract

In this paper we report the synthesis of new A_1/A_3 adenosine receptor antagonists designed as simplification products of the A_1 antagonists with pyrazolo[1′,5′:1,6]pyrimido[4,5-d]pyridazin-4(3H)-one scaffold previously published by us. Preliminary screening with NanoBRET competition binding assay revealed a number of products with pKi ≥ 5 for A_1R and A_3R, and on some representative compounds the antagonist profile as well as their selectivity versus $A_{2A}R$ and $A_{2B}R$ have been validated by antagonizing **NECA** in cAMP accumulation. The most interesting compounds resulted the A_1/A_3 mixed antagonist **3b** (pKi = 6.41 and 6.29 for A_1R and A_3R respectively) and the selective A_3R antagonist **5c** (pKi = 6.40). Furthermore, *in silico* simulations were carried out to study the molecular mechanism of the high affinity of **3b** for A1/A3R as well as the selectivity of **5c** for A_3R over A_1R.

Keywords: G Protein-Coupled Receptor, Adenosine Receptor, Antagonist, BRET, Binding, cAMP, docking

1. Introduction

Adenosine receptors (ARs) are membrane receptors widely distributed in various tissues and organs throughout the body. They are a sub-family of Class A G protein-coupled receptors (GPCRs), classically consisting of seven transmembrane α helices connected to each other by three intracellular and three extracellular loops [1]. There are four AR subtypes, namely A_1R, $A_{2A}R$, $A_{2B}R$ and A_3R. A_1R and A_3R interact with the $G\alpha_{i/o}$ family of G proteins, inhibiting adenylyl cyclase, thus reducing the production of cAMP, while $A_{2A}R$ and $A_{2B}R$ stimulate the production of cAMP by interacting with $G\alpha_s$ proteins [2,3].

Since their discovery and validation as pharmacological targets in the 1980s', ARs have been the focus of intensive drug discovery programs, in the context of a plethora of different conditions, for instance cancer, asthma, infant apnea [4], renal injury [5], immune system disorders [6] and cardiovascular disease (e.g. cardiac arrhythmias and coronary dysfunction) [7,8]. Recently, ARs have also been investigated for their potential involvement in the resolution of Covid-19 disease-associated pneumonia and lung inflammation. The use of inhaled adenosine demonstrated improvements in oxygenation levels in Covid-19 patients, leading to the protection of lungs from inflammatory damage, and a rapid improvement of the overall clinical condition [9,10]. Nonetheless, AR modulation in the treatment of Alzheimer's and Parkinson's disease, as well as other central nervous system (CNS) disorders [11,12], remains one of the most active fields to identify new clinical approaches for neurodegenerative conditions. Regarding the latter, A_1Rs have been found widely distributed throughout the CNS, with particularly high expression in brain tissue, notably the hippocampus, cerebral cortex, and cerebellum [13]. Several A_1R antagonists have demonstrated positive therapeutic effects on various neurological contexts and pathologies, such as the ability to inhibit β amyloid toxicity in cerebellar granule neurons in mouse models of Alzheimer's disease (AD) [14,15]. Elevation of both A_1R and $A_{2A}R$ levels and sensitivity has been also observed in the frontal cortex and hippocampus of AD patients [12,16]. Moreover, it has been widely demonstrated that increased Aβ and phosphorylated Tau protein levels are factors that can lead to neurotoxicity.

Noteworthy, A_1R knockout mice have been found to reverse this effect, thereby ameliorating cognitive impairment [17,18]. In this regard, selective A_1R antagonists are promising therapeutic targets in AD and for the treatment of cognitive deficits. On the other hand, although A_3R show a low sequence identity among species, in particular rodents versus primates [19], they have proven to be an interesting target for some years for agonists and antagonists [20]. In particular, selective A_3R antagonists have been recently developed reaching clinical trials for the treatment of glaucoma, ulcerative colitis, psoriasis, and Nonalcoholic Steatohepatitis (NASH) [2,21]. Moreover, A_3R antagonists have been shown to be useful in animal models of brain ischemia [20] and across different cancer types [22].

Overall, given their high structural and sequence homology and their wide, sometimes overlapping, tissue and organ distribution, the development of selective ligands (e.g. containing a modified nucleoside scaffold of adenosine, as well as small molecules which could act as both active site and/or allosteric modulators) remains both challenging and imperative [23]. Activation of multiple signaling pathways, potential off target side effects, and low subtype selectivity are typical limitations in the development of AR ligands, with the latter two serious challenges for the development of antagonists [24]. Thus, focusing on structural modification of established AR binders is a valid approach to identify drug candidates with enhanced efficacy and selectivity, and to facilitate a possible translation into clinical settings [25].

Here, we describe the development of a new series of high affinity A_1R/A_3R mixed antagonists as further elaboration of already identified heterocyclic hits. More in detail, based on Jacobson's structural requirements for molecules leading to effective AR binding (i.e. planar, aromatic or π electron rich and nitrogen-containing heterocycles) [13], we have previously developed a series of tricyclic compounds, with a pyrazolo[1′,5′:1,6]pyrimido[4,5-d]pyridazin-4(3H)-one scaffold [26-28], possessing all the necessary features to bind ARs effectively. Within this series, we recorded interesting biological results towards A_1R in terms of both affinity and selectivity. This led to the

identification of a potent and selective A_1R antagonist (compound **A**, **Figure 1**), which was also further assessed *in vivo* through the mouse passive avoidance model, exhibiting relevant anti-amnesic effects [26]. By adopting compound **A** as the lead compound, we report here the molecular simplification design of a new series of AR antagonists, expected to possess suitable potency and isoform selectivity, along with improved overall physical-chemical properties (e.g. high solubility in biological fluids, increased capability to cross membranes), to facilitate biological and pharmacological applications. Specifically, we have simplified the tricyclic structure of the original ligand (e.g. compound **A**) through the development of 6/6- and 6/5-bicyclic compounds (i.e. based on pyrimido[4,5-d]pyridazine-4,8-dione and pyrazolo[1,5-a]pyrimidine-7-one scaffolds, **B** and **C**, respectively, in **Figure 1**). Moreover, we have also explored additional bicyclic templates (i.e. pyrrolo[1,2-a]pyrimidine, 1,8-naphtyridine and pyrido[1,2-a]pyrimidine) as possible *core* scaffolds to further develop antagonists towards ARs. In the new bicyclic series developed herein, we have maintained the essential structural requirements (of both scaffold and side-chain residues) for AR binding (see **Figure 1**), following the structural analysis of selected hit compounds previously developed by us and/or present in the literature.

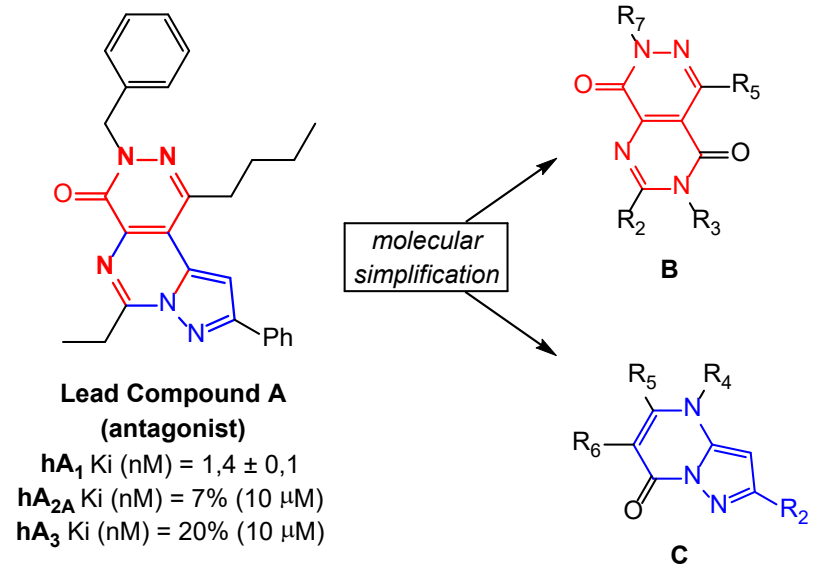

Figure 1. The antagonist lead compound **A** and the structural simplification approach explored in this work (scaffold **B** and **C**).

2. Results and discussion

2.1. Chemistry

The products reported in this study are bicycles with pyrazolo[1,5-a]pyrimidine and pyrimido[4,5-d]pyridazine scaffold as simplification of the pyrazolo[1′,5′:1,6]pyrimido[4,5-d]pyridazin-4(3H)-one structure of the lead compound **A**, but also pyrrolo[1,2-a]pyrimidines, 1,8-naphtyridines and pyrido[1,2-a]pyrimidines and the synthesis of the new products is depicted in **Schemes 1-9**. All the final compounds of type **1-5** (**1b** [29], **1m, 1n** [30], **2b** [31], **3b** [32], **4a** and **4c** [33]) have been tested as adenosine receptors ligands (see **Tables 1** and **2** of chemical structures).

The synthesis of pyrazolo[1,5-a]pyrimidine derivatives **1a-n** and **2a-c** is reported in **Schemes 1-5**.

Scheme 1 depicts the cyclization of commercially available 3-phenyl-5-amino-1H-pyrazole **6** with the appropriate ester derivatives, in ethanol/acetic acid to afford the final 6-ethyl-2-phenylpyrazolo[1,5-a]pyrimidin-7(4H)-one **1a** and intermediate **7**, differently substituted at position 5 and 6.

The 2-phenylpyrazolo[1,5-a]pyrimidin-7(4H)-ones **1b** [29]**, 7**, **8** [29] and **9** [34] were reacted in classical conditions with methyl iodide affording **1c** (from **1b**), with H_2SO_4/HNO_3 affording **1d,e** (from **1b** and **8** respectively) and with NBS/CH_2Cl_2 yielding compounds **1f** and **1g** (from **1b** and **7**). Instead, the treatment of compound **9** with bromine gave the 3,6-dibromo derivative 3,6-dibromo-5-methyl-2-phenylpyrazolo[1,5-a]pyrimidin-7(4H)-one **1h**. Next, on the two ester derivatives **1d** and **1f** an alkaline hydrolysis in 10% NaOH was performed obtaining the corresponding 6-carboxylic acid, **1i** and **1j** (after acidification) (**Scheme 2**).

The final amino derivative **1k** was obtained starting from the 5-methyl-3-nitroso-2-phenylpyrazolo[1,5-a]pyrimidin-7(4H)-one **10** [35], easily reduced in the Parr equipment (H_2-Pd/C, 30 PSI) to the 3-amino derivative **11**, which gave the desired 3-benzylideneamino derivative **1k** by treatment with benzaldehyde (**Scheme 3**).

The synthesis of the 6-cyano-3-phenylpyrazolo[1,5-a]pyrimidin-7(4H)-one **1l** (**Scheme 4**) was carried out with the commercially available 4-phenyl-5-aminopyrazole **12** and ethyl 2-cyano-3-oxopropanoate **13** into a mixture of acetic acid/ethanol.

S**cheme 5** reports the chemical procedure to obtain 6-acetyl-7-methyl-3-phenylpyrazolo[1,5-a]pyrimidin-2(1H)-one **2a** starting from the commercial product **14**, by rapid cyclization with ethoxymethylenacetylacetone in ethanol/HCl. Differently, compound **2b** [31] undergoes the N-alkylation in standard conditions (DMF/K_2CO_3/MeI), to give **2c** in good yield.

In **Scheme 6** is reported the synthesis of the new pyrrolo[1,2-a]pyrimidine derivative **3a** obtained by treatment of ethyl 8-cyano-4-oxo-7-phenyl-1,4-dihydropyrrolo[1,2-a]pyrimidine-3-carboxylate **15** [36] with Lawesson's reagent in usual conditions.

The synthesis of the final compounds **4a-c** with pyrimido[4,5-d]pyridazine scaffold is reported in **Scheme 7**. Starting from the 4-amino-5-amido derivatives **16a,b** [33], the standard alkylation with suitable alkyl(aryl) halides afforded the intermediates **17a-c** (**17a,c** [33]) which were treated with triethylorthoformate in H_2SO_4 at high temperature to afford compounds **4a-c** (**4a,c** [33]).

In the **Scheme 8** is depicted the procedure to obtain the naphthyridone derivatives as type **5**. Starting from intermediate **18** [33], the final **5a** and the intermediate **19a** [33] were obtained through standard alkylation reaction with the suitable alkyl halide, while the coupling reaction with phenyl boronic acid and copper acetate in dry dichloromethane generated the product **19b** [33]. The alkaline hydrolysis of the ester group in compounds **19a,b** afforded the carboxylic acids **20a,b** [33] which were firstly converted into the corresponding acid chlorides using $SOCl_2$ at room temperature and then treated with the appropriate (hetero)arylamine in dry tetrahydrofuran to give the final compounds **5b,c**. Lastly, the pyrido[1,2-a]pyrimidine derivative **5d** was obtained using the same procedure reported in **Scheme 8**, but starting from intermediate **21** [33] and using N-methylaniline as reagent (**Scheme 9**).

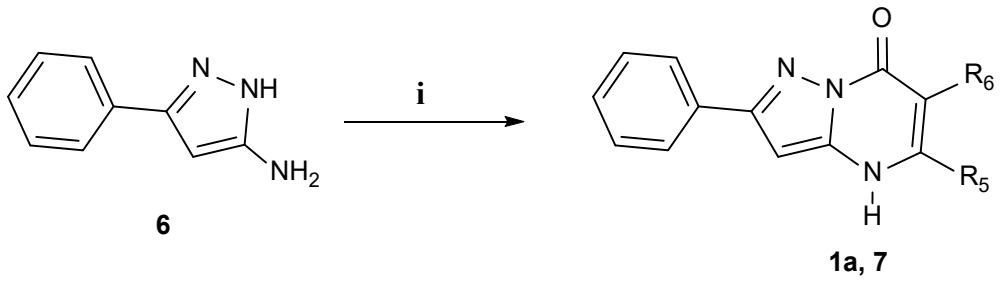

6

1a, 7

Comp.	R_5	R_6
1a	H	CH_2CH_3
7	CH_3	CH_3

Scheme 1. Reagents and conditions: i) EtOH/acetic acid, ethyl formylbutanoate (**for 1a**) or ethyl 2-methyl-3-oxobutanoate (**for 7**), reflux, 10 min.

Comp.	R_4	R_5	R_6
1b	H	H	COOEt
7	H	CH_3	CH_3
8	CH_3	H	H
9	H	CH_3	H

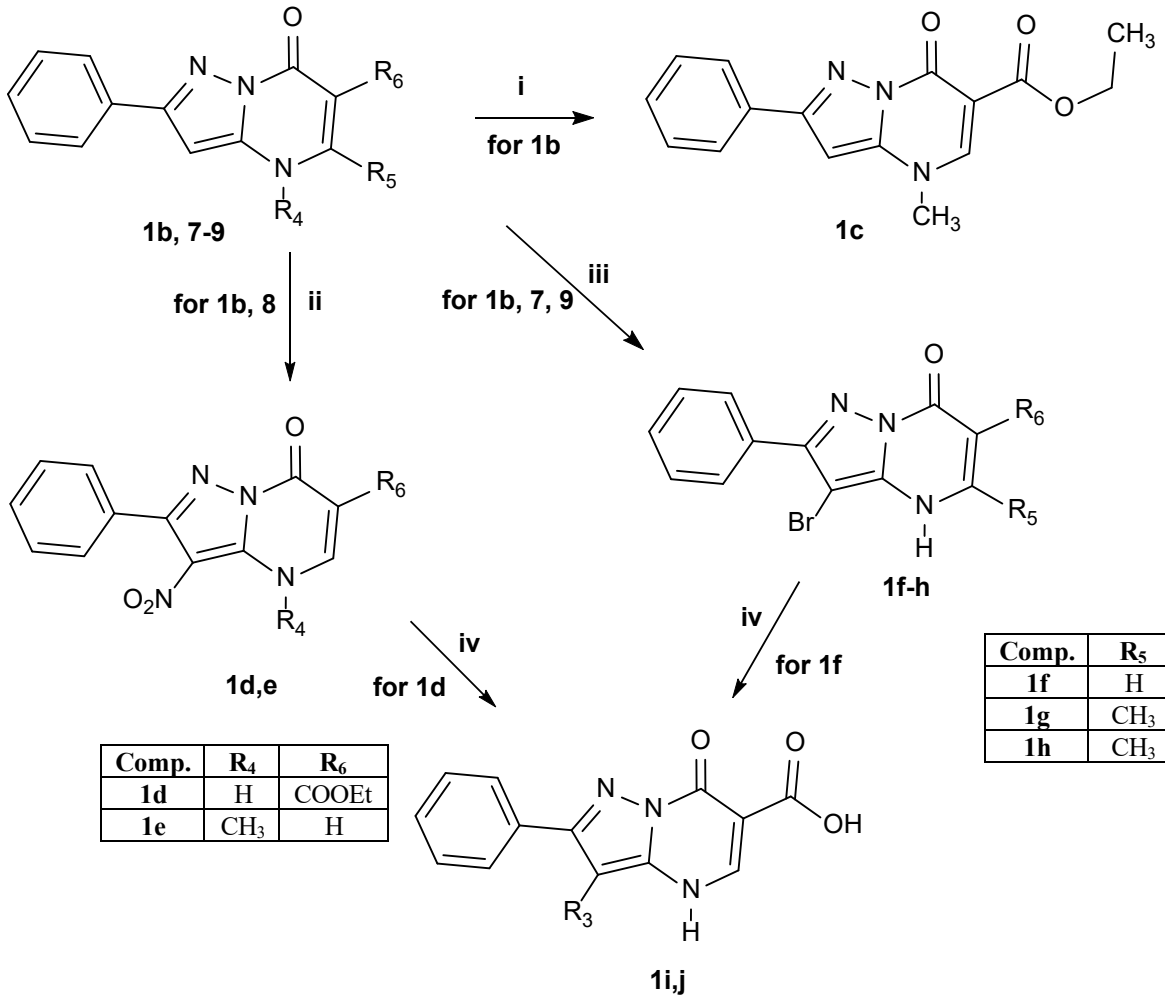

Comp.	R_4	R_6
1d	H	COOEt
1e	CH_3	H

Comp.	R_5	R_6
1f	H	COOEt
1g	CH_3	CH_3
1h	CH_3	Br

Comp.	R_3
1i	NO_2
1j	Br

Scheme 2. Reagents and conditions: i) DMF anhydrous/K_2CO_3/MeI, 40 °C, 2 h; **ii)** glacial acetic acid, HNO_3 fuming/H_2SO_4 conc, 20 °C, 30 min; **iii) 1b** (for **1f**) or **7** (for **1g**), NBS, CH_2Cl_2, rt, 1 h; **9** (for **1h**) Br_2/acetic acid, reflux, 1 h; **iv)** 10% NaOH, rt, 1-2 h.

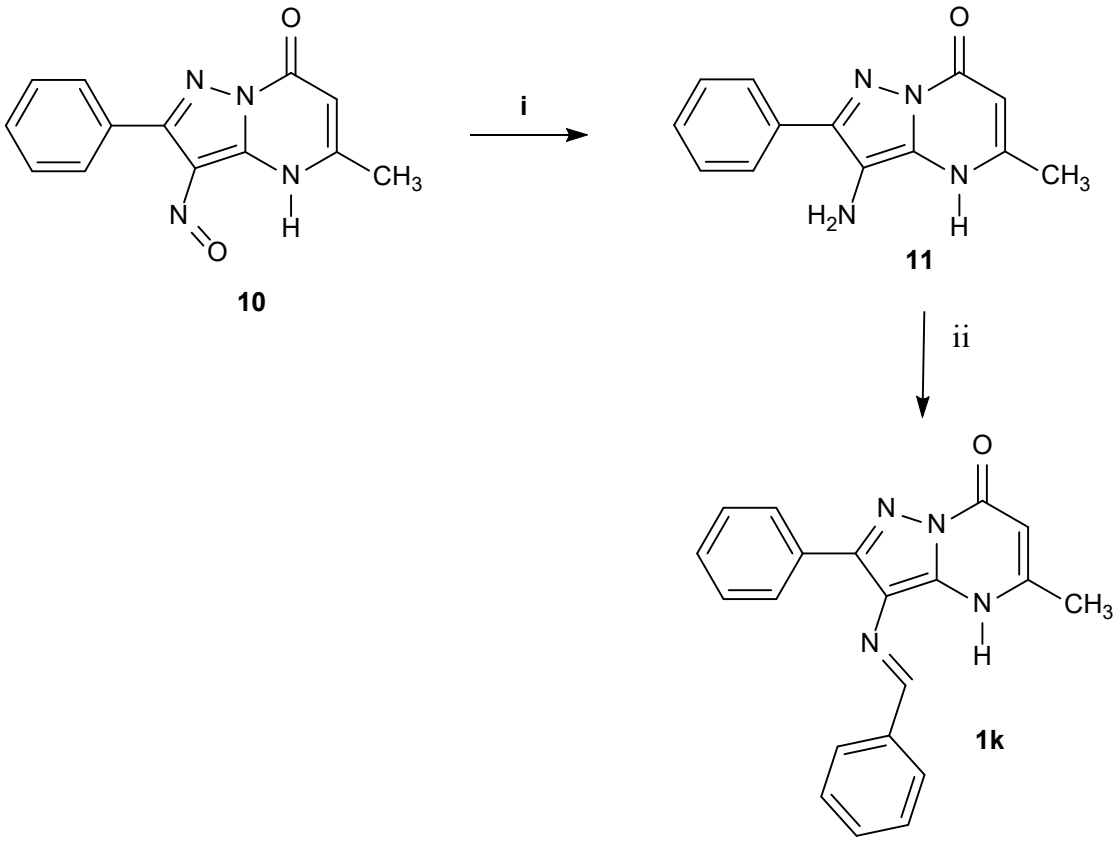

Scheme 3. Reagent and conditions: i) Parr equipment, EtOH, H_2-Pd/C, 2 h; **ii)** EtOH, benzaldehyde, p-TSA, 10 min, rt.

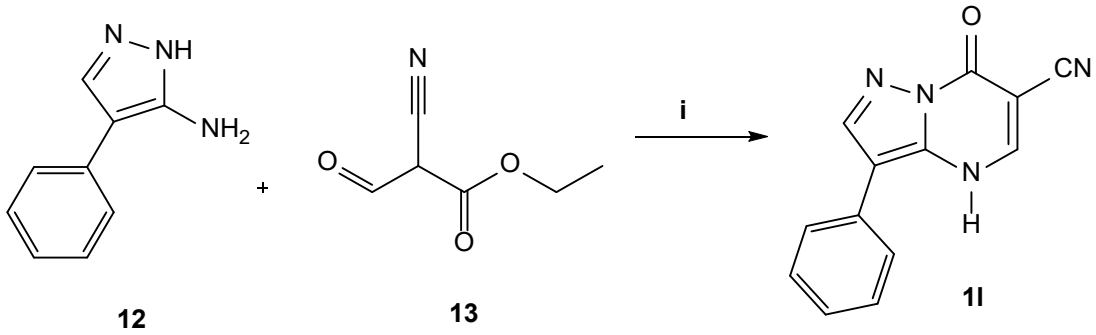

Scheme 4. Reagent and conditions: i) EtOH/acetic acid, reflux, 30 min.

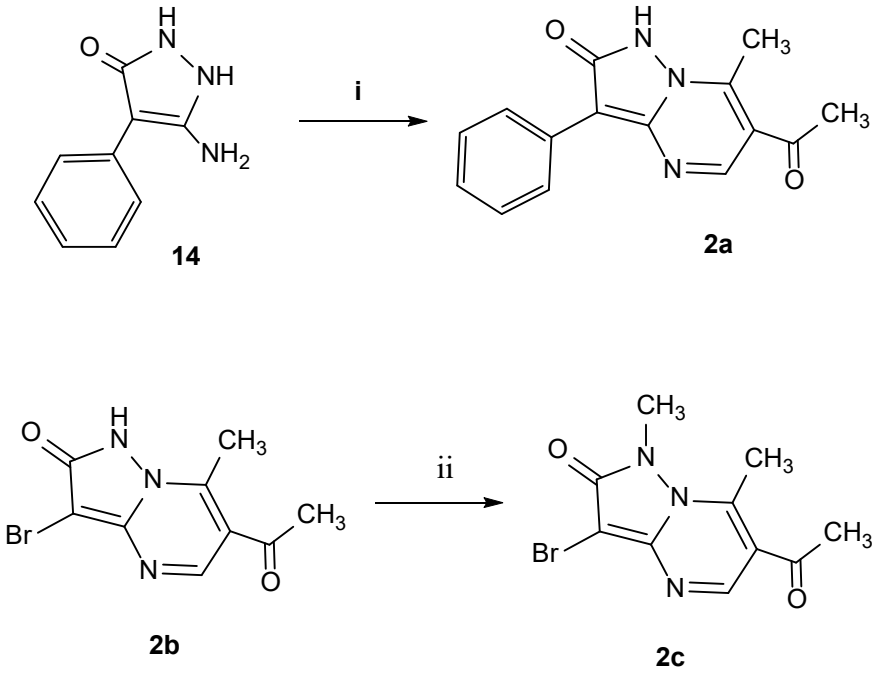

Scheme 5. Reagents and conditions: i) ethoxymethylenacetylacetone, 2N HCl, ethanol, 60 °C, 0.5 h; **ii)** anhydrous DMF, K_2CO_3, MeI, 50 °C, 2 h.

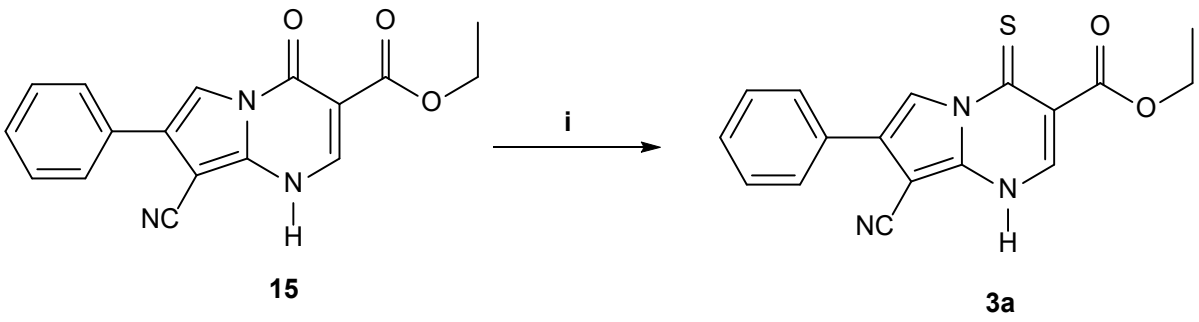

Scheme 6. Reagent and conditions: i) Lawesson's reagent, toluene, reflux, 6 h.

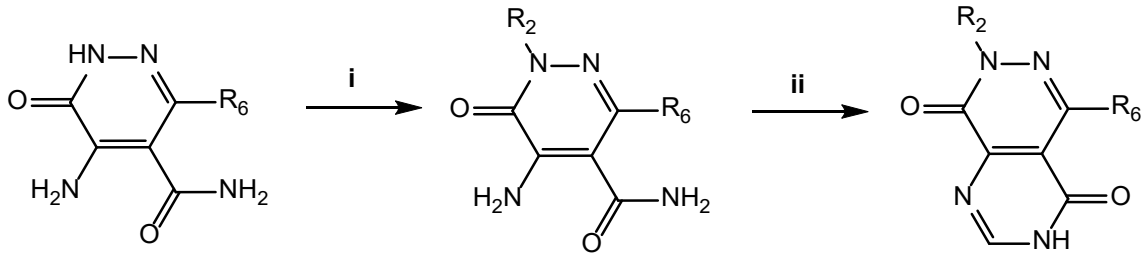

16a,b 17a-c 4a-c

16	R_6
a	Ph
b	3-Cl-Ph

Comp.	R_6	R_2
17a/4a	Ph	CH_2CH_3
17b/4b	3-Cl-Ph	$CH_2cC_5H_9$
17c/4c	3-Cl-Ph	cC_6H_{11}

Scheme 7. Reagents and conditions: i) suitable alkyl(aryl) halide, K_2CO_3, DMF, 80 °C, 1-3 h; **ii)** triethylorthoformate, H_2SO_4 conc, 130 °C, 1-5 h.

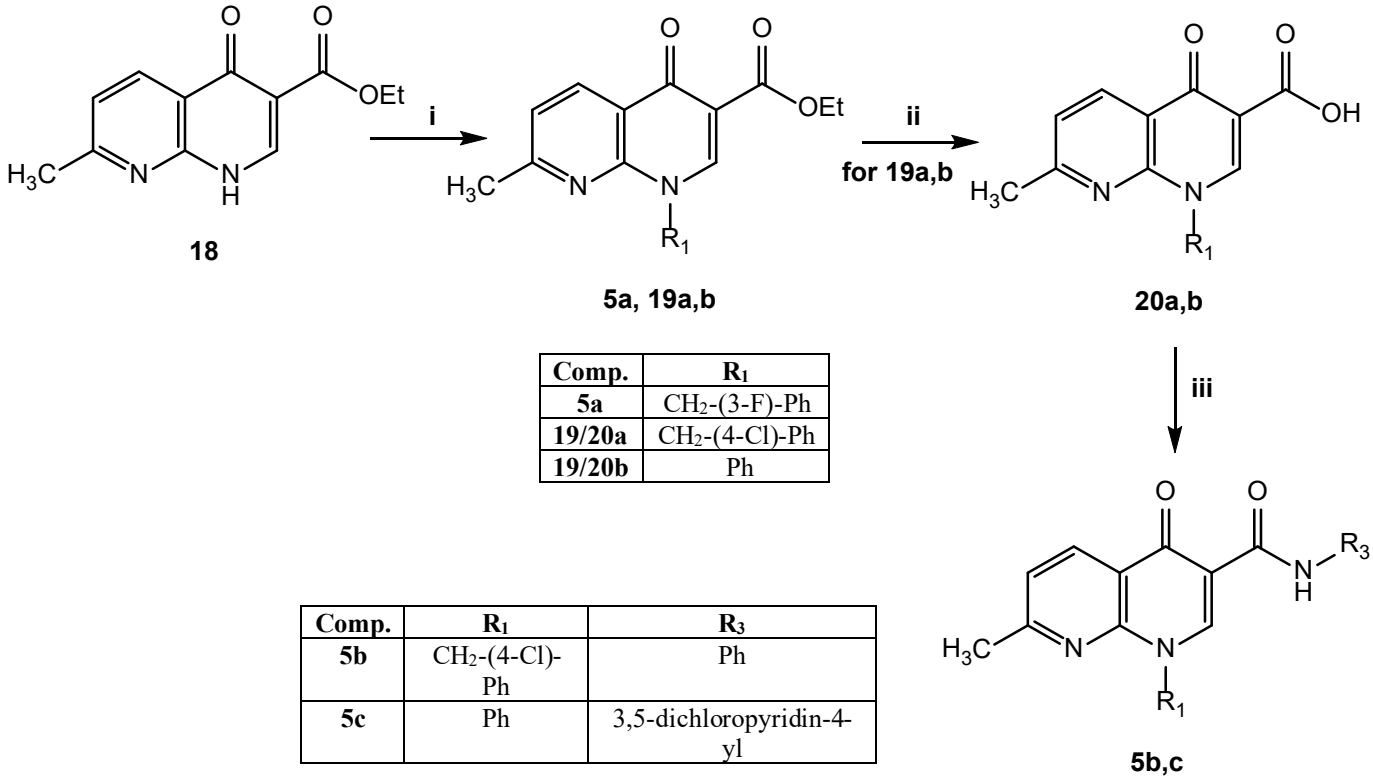

18 5a, 19a,b 20a,b 5b,c

Comp.	R_1
5a	CH_2-(3-F)-Ph
19/20a	CH_2-(4-Cl)-Ph
19/20b	Ph

Comp.	R_1	R_3
5b	CH_2-(4-Cl)-Ph	Ph
5c	Ph	3,5-dichloropyridin-4-yl

Scheme 8. Reagents and conditions: i) for 5a and 19a, suitable R-benzyl bromide, K_2CO_3, DMF, 80 °C, 1-3 h; **for 19b**, phenylboronic acid, dry CH_2Cl_2, $Cu(Ac)_2$, Et_3N, rt, 24 h; **ii)** 6N NaOH, EtOH, rt, 0.5-1 h; **iii) for 5b**, step 1: $SOCl_2$, **20a**, Et_3N, rt, 2-3 h; step 2: aniline, anhydrous THF, rt, 2-3 h; **for 5c**, step 1: $SOCl_2$ (excess), **20b**, Et_3N (catalytic), rt, 2-3 h; step 2: 3,5-dichloro-4-pyridilamine, NaH, anhydrous THF, rt, 30 min.

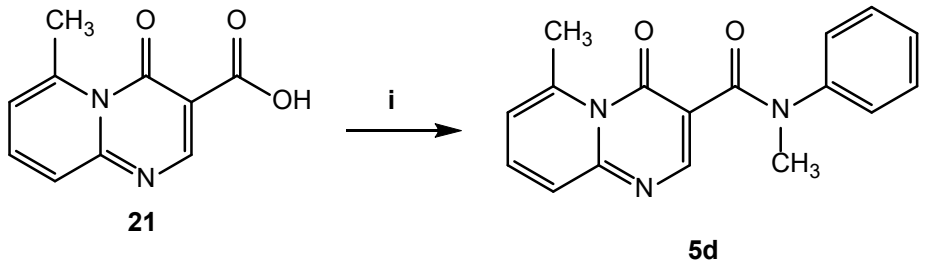

Scheme 9. Reagents and conditions: i) step 1: $SOCl_2$, Et_3N, rt, 2-3 h; step 2: *N*-methylaniline, anhydrous THF, rt, 2-3 h.

2.2. Pharmacological Activity

2.2.1. Affinity Measurement using a NanoBRET Binding Assay

Following synthesis and purification we first studied all the final compounds (**Table 1** and **2**) to assess their binding affinity for A_1R and A_3R using a previously described NanoBRET competition binding assay where the fluorescent antagonist CA200645, having high affinity for both receptors, was used as a tracer [37,38].

Table 1. Chemical structure of compounds with pyrazolo[1,5-a]pyrimidine scaffold (**1a-n** and **2a-c**).

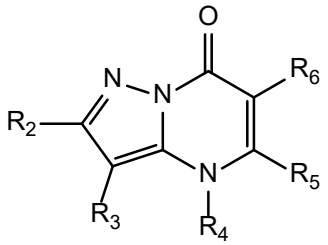

1a-n

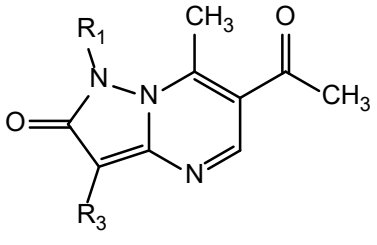

2a-c

Compounds	R_6	R_5	R_4	R_3	R_2	R_1
1a	CH_2CH_3	H	H	H	Ph	-
1b [29]	COOEt	H	H	H	Ph	-
1c	COOEt	H	CH_3	H	Ph	-
1d	COOEt	H	H	NO_2	Ph	-
1e	H	H	CH_3	NO_2	Ph	-
1f	COOEt	H	H	Br	Ph	-
1g	CH_3	CH_3	H	Br	Ph	-
1h	Br	CH_3	H	Br	Ph	-
1i	COOH	H	H	NO_2	Ph	-

1j	COOH	H	H	Br	Ph	-
1k	H	CH_3	H	-N=C-Ph	Ph	-
1l	CN	H	H	Ph	H	-
1m [30]	CH_3	H	H	H	Ph	-
1n [30]	H	COOH	CH_3	H	Ph	-
2a	-	-	-	Ph	-	H
2b [31]	-	-	-	Br	-	H
2c	-	-	-	Br	-	CH_3

Table 2. Chemical structure of compounds with pyrrolo[1,2-a]pyrimidine (**3a,b**), pyrimido[4,5-d]pyridazine (**4a-c**), 1,8-naphtyridine (**5a-c**) and pyrido[1,2-a]pyrimidine (**5d**) scaffold.

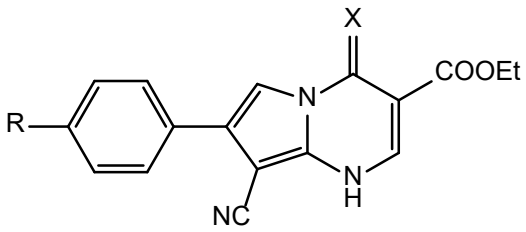

3a,b

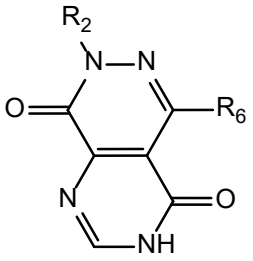

4a-c

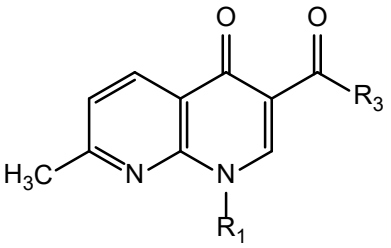

5a-c

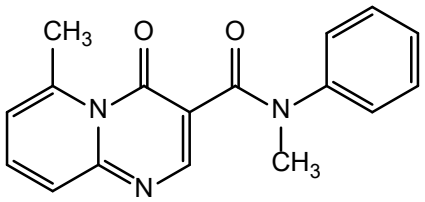

5d

Comp.	X	R	R_1	R_2	R_3	R_6
3a	S	H	-	-	-	-
3b [32]	O	Cl	-	-	-	-
4a [33]	-	-	-	CH_2CH_3	-	Ph
4b	-	-	-	$CH_2cC_5H_9$	-	3-Cl-Ph
4c [33]	-	-	-	cC_6H_{11}	-	3-Cl-Ph
5a	-	-	CH_2-3-F-Ph	-	OEt	-
5b	-	-	CH_2-4-Cl-Ph	-	NH-Ph	-
5c	-	-	Ph	-	NH-(3,5-dichloropyridin)-4-yl	-
5d	-	-	-	-	-	-

The compounds with a pyrazolo[1,5-a]pyrimidine scaffold, displayed low affinities for both receptors with the highest being **1e** and **1l** (**Figure 2A**, **Table 3**). Whereas **1e** showed selectivity towards the

A_3R (pKi of 4.26 ± 0.40 for A_1R and 5.51 ± 0.13 for A_3R), **1l** was non-selective (pKi of 5.11 ± 0.25 and 5.35 ± 0.05 for A_1R and A_3R respectively). Similarly, compounds with a pyrazolo[1,5-a]pyrimidin-2(1*H*) scaffold also showed low affinity, with **2b** displaying the highest affinity, with a pKi of 5.29 ± 0.23 for A_1R (**Figure 2B**, **Table 3**). Both **1e** and **2b**, whilst having appreciable calculated pKi values at A_3R, showed incomplete displacement of CA200645, and were subsequently deemed of low affinity (see Figure SF1, in Supporting Information).

Compounds with a pyrrolo[1,2-a]pyrimidine scaffold showed the highest affinities among different scaffolds (**Figure 2C**, **Table 3**), with both **3a** and **3b** displaying a pKi above 5 for both receptors; **3a** had affinities of 5.51 ± 0.14 and 5.03 ± 0.28, and **3b** 6.41 ± 0.12 and 6.29 ± 0.13 for A_1R and A_3R respectively. Neither showed selectivity, but **3b** did display the highest affinity for A_1R of all the compounds tested, similar to that of the non-selective agonist 5'-N-Ethylcarboxamidoadenosine (**NECA**).

Among those with a pyrimido[4,5-d]pyridazine scaffold, both **4b** and **4c** displayed moderate affinity for A_1R (5.34 ± 0.13 and 5.53 ± 0.10 respectively), and slightly higher affinity for A_3R (pKi of 5.70 ± 0.06 and 6.00 ± 0.12 respectively). **4a**, however, was unable to bind to either receptor (**Figure 2D**, **Table 3**).

Within the final set of compounds, **5d** showed no measurable affinity for A_3R, and only low affinity for A_1R (pKi of 4.60 ± 0.13) (**Figure 2E**, **Table 3**). However, the remaining three compounds displayed some selectivity towards the A_3R. **5a** had a pKi of 5.13 ± 0.13 for A_3R, and no determinable affinity for A_1R. Both **5b** and **5c** had moderate affinities for A_1R (pKi of 5.56 ± 0.18 and 4.72 ± 0.49 respectively), but displayed micromolar affinities for the A_3R (pKi of 6.28 ± 0.12 and 6.40 ± 0.04 respectively). **5c** had the highest affinity for the A_3R of all compounds tested.

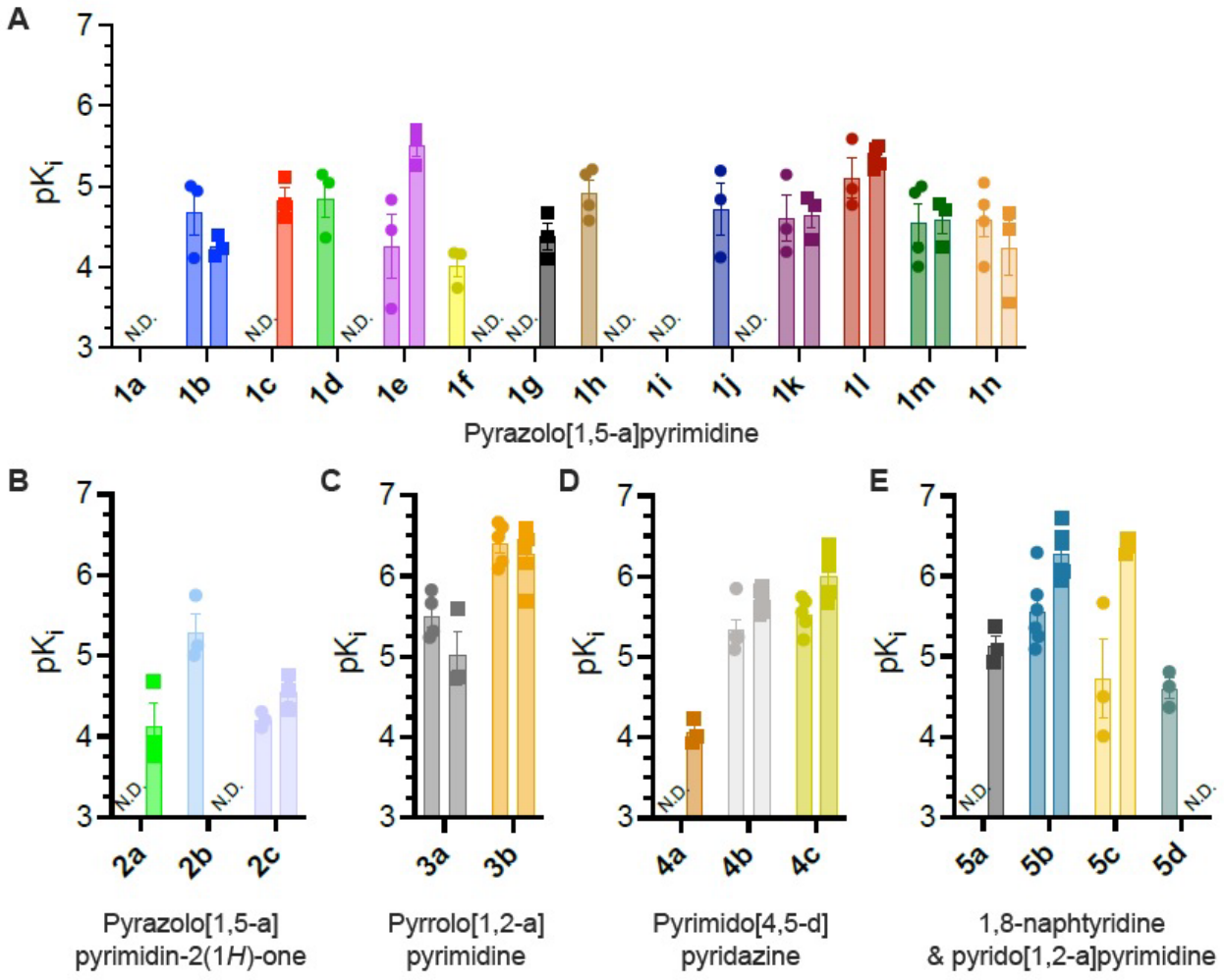

Figure 2. pKi values for compounds tested with NanoBRET competition binding assay, in HEK293 cells expressing Nluc-A_1R (circles) or Nluc-A_3R (squares). Values are plotted from individual replicates with error bars to indicate mean±SEM. N.D. indicates where no pK_i could be determined.

Table 3. pKi values of all the final compounds at A_1R and A_3R (determined through NanoBRET ligand binding).

	A_1R	**A_3R**
	Pyrazolo[1,5-a]pyrimidine	
Compound	**pK_i** [a]	**pK_i** [a]
1a	N.D.[b]	N.D.[b]
1b	4.69 ± 0.29	4.26 ± 0.08
1c	N.D.[b]	4.84 ± 0.15
1d	4.86 ± 0.25	N.D.[b]
1e	4.26 ± 0.40	5.51 ± 0.13
1f	4.03 ± 0.14	N.D.[b]
1g	N.D. [b]	4.38 ± 0.16
1h	4.93 ± 0.15	N.D.[b]
1i	N.D.[b]	N.D.[b]
1j	4.72 ± 0.32	N.D.[b]
1k	4.61 ± 0.28	4.66 ± 0.16
1l	5.11 ± 0.25	5.35 ± 0.05
1m	4.55 ± 0.25	4.58 ± 0.17
1n	4.60 ± 0.22	4.24 ± 0.34
	Pyrazolo[1,5-a]pyrimidin-2(1*H*)one	
2a	N.D.[b]	4.12 ± 0.28
2b	5.29 ± 0.23	N.D.[b]
2c	4.21 ± 0.06	4.56 ± 0.12
	Pyrrolo[1,2-a]pyrimidine	
3a	5.51 ± 0.014	5.13 ± 0.28
3b	6.41 ± 0.12	6.29 ± 0.13
	Pyrimido[4,5-d]pyridazine	
4a	N.D.[b]	4.06 ± 0.09
4b	5.34 ± 0.13	5.70 ± 0.06
4c	5.53 ± 0.10	6.01 ± 0.12
	1,8-naphtyridine and pyrido[1,2-a]pyrimidine	
5a	N.D.[b]	5.13 ± 0.13
5b	5.56 ± 0.18	6.28 ± 0.12
5c	4.72 ± 0.49	6.40 ± 0.04
5d	4.60 ± 0.13	N.D.[b]

[a]pKi values are reported ± SEM and represent the mean of 3-6 experiments; [b]N.D. = Not Determined.

2.2.2. *Validating the novel scaffolds as Adenosine Receptor Antagonists*

To validate these novel compounds as adenosine receptor antagonists, cells expressing either A_1R or A_3R were treated with a fixed concentration of compound (10μM) and increasing concentrations of the agonist **NECA** and the inhibition of forskolin-evoked cAMP was measured. Only those which displayed moderate affinity at either receptor were carried forward: **1l, 3a, 3b, 4b, 4c, 5b** and **5c.**

All compounds were shown to reduce the potency of **NECA**-mediated inhibition of forskolin-stimulated cAMP at least one receptor subtype, confirming their activity as antagonists (**Figure 3A**, **Table 4**). Using the Schild equation [39], affinities could also be calculated from the cAMP accumulation assays, giving pKb values [38]. For **1l**, **4b**, **4c**, and **5c**, there was good agreement between the pKi and pKb values (**Figure 3B**). No pKb value could be calculated for **3a** at A_3R, likely due to its lower affinity at this receptor. Despite showing high affinity for A_1R in the binding assay, a pKb could not be calculated for **5b** suggesting a lack of functional affinity at A_1R. For both A_1R and A_3R, the pKb calculated for **3b** were lower than the pki.

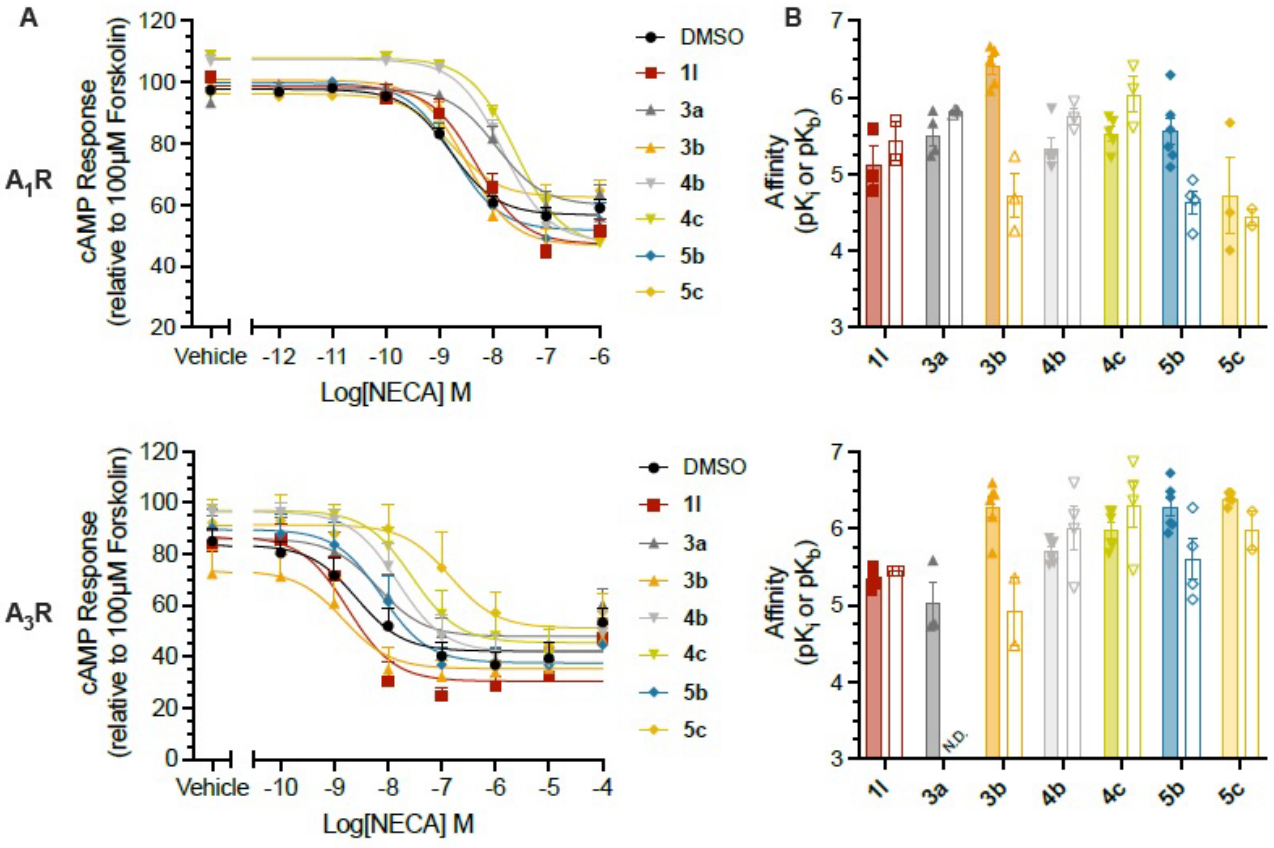

Figure 3. All high affinity compounds were demonstrated to be antagonists of the inhibitory ARs. Inhibition of cAMP accumulation at A_1R (upper) and A_3R (lower), in response to NECA, in the absence or presence of test compounds. (A) Dose response curves, showing antagonism of the response by compounds. Values are plotted as mean, of n repeats, with error bars to indicate the SEM, where n is between 3 and 7. (B) comparison of pKi (solid bars and symbols) and pKb values (open bars and symbols) calculated from binding and cAMP respectively. Values from individual replicates are plotted, with error bars in indicate mean±SEM. N.D. Indicates where no pKb could be calculated.

Table 4. pEC_{50} and pK_b values for the inhibition of forskolin-evoked cAMP accumulation by NECA in CHO-K1 cells expressing A_1R or A_3R, in the presence of DMSO or test antagonists.

	A_1R		**A_3R**	
Compound	**pEC_{50}[a]**	**pK_b[a]**	**pEC_{50}[a]**	**pK_b[a]**
DMSO	8.76 ± 0.07	N.A.[b]	8.53 ± 0.27	N.A.[b]
1l	8.44 ± 0.20	5.44 ± 0.25	8.75 ± 0.14	5.45 ± 0.00
3a	7.91 ± 0.08	5.81 ± 0.02	8.26 ± 0.28	N.D.[c]
3c	8.49 ± 0.03	4.73 ± 0.28	8.84 ± 0.23	4.92 ± 0.44
4b	7.89 ± 0.10	5.75 ± 0.11	7.80 ± 0.26	6.00 ± 0.29
4c	7.63 ± 0.09	6.04 ± 0.24	7.52 ± 0.26	6.31 ± 0.30
5b	8.73 ± 0.08	4.63 ± 0.15	8.14 ± 0.25	5.60 ± 0.27
5c	8.72 ± 0.13	4.44 ± 0.11	6.87 ± 0.27	5.98 ± 0.25

[a]Values are reported as mean ± SEM and represent the mean of 3-7 experiments; pEC_{50} of individual replicates were used to calculate pK_b values, using the Schild equation; [b]N.A. = Not applicable. [c]N.D. = Not determined.

2.2.3. Confirming selectivity across the Adenosine Receptor Family

The adenosine receptor family shows high conservation, with each family member at least 30% identical to any other. Whilst many of the compounds tested showed some selectivity between A_1R and A_3R, some did not, and most bound to both receptors. The next step was to confirm selectivity of the lead compounds against $A_{2A}R$ and $A_{2B}R$, which are often co-expressed with A_1R or A_3R and have opposing signaling cascades. To determine binding at these receptors, the ability of the compounds to antagonize **NECA** in cAMP accumulation was again used (**Figure 4A-B**, **Table 5**) although since the $A_{2A}R$ and $A_{2B}R$ are both coupled to the stimulatory G protein addition of forskolin was not required. Many of the antagonists reduced the potency of **NECA** at $A_{2A}R$ and $A_{2B}R$ (**Figure 4C**), enabling pK_b values to be calculated (**Figure 4D**). **4b** did not bind either $A_{2A}R$ or $A_{2B}R$, showing selectivity for the inhibitory adenosine receptors (**Figure 4C**). Whilst **5c** also maintained selectivity,

selectively antagonizing the A_3R, **5b** showed reduced selectivity, with similar pK_b's values for the A_3R and $A_{2B}R$.

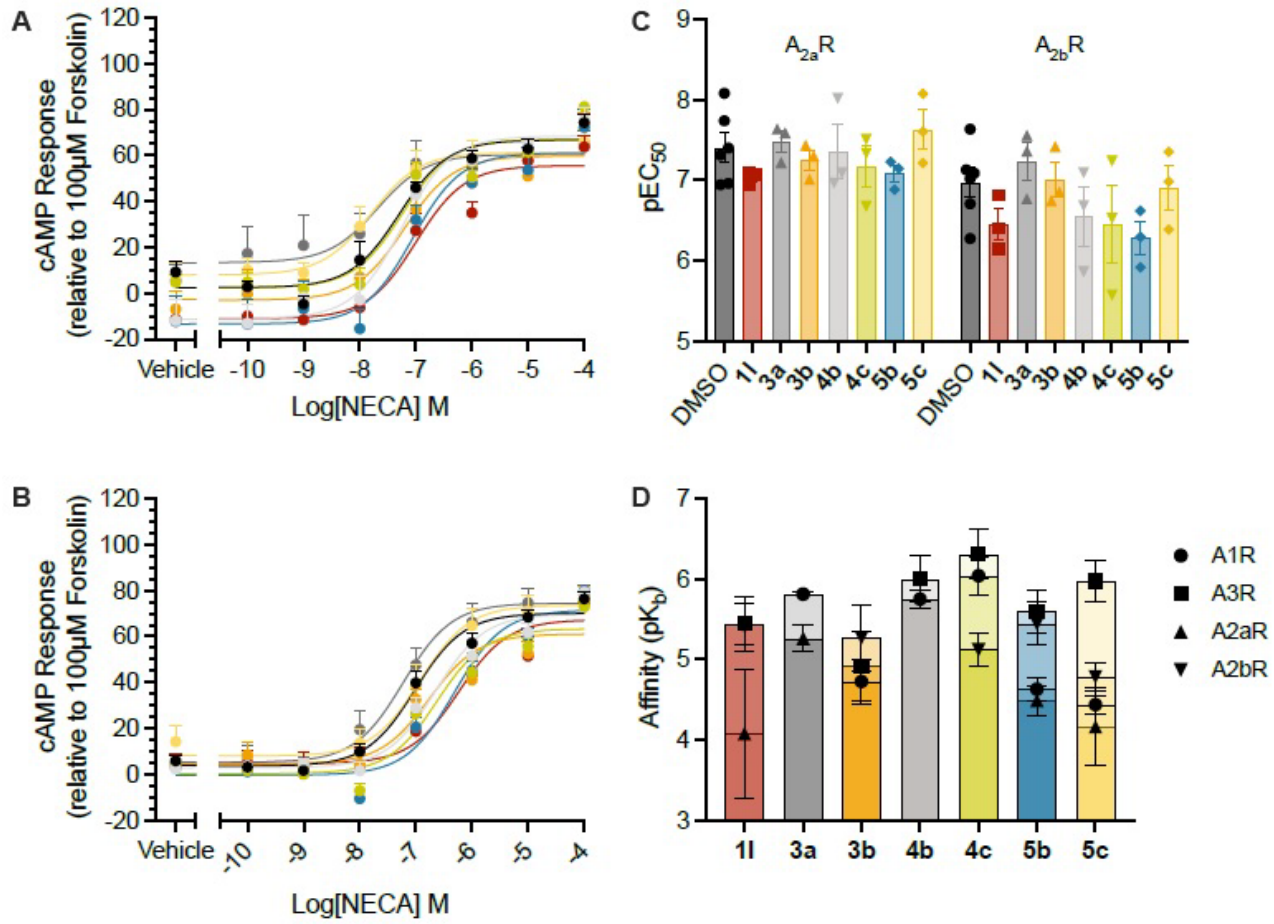

Figure 4. Varied selectivity of the compound series for the inhibitory adenosine receptors. Antagonism of NECA-evoked cAMP accumulation in CHO-K1 cells expressing the $A_{2A}R$ (A) or $A_{2B}R$ (B). pEC_{50} values when the compounds were present (C) were used to calculated pK_b values (D) for all ARs (A_1R• or A_3R▪) or accumulation ($A_{2A}R$▲ and $A_{2B}R$▼). Values are plotted as mean±SEM.

Table 5. pEC_{50} and pK_b values for cAMP accumulation mediated by NECA in CHO-K1 cells expressing the $A_{2A}R$ or $A_{2B}R$, in the presence of DMSO or test antagonists.

	$A_{2A}R$		**$A_{2B}R$**	
Compound	**pEC_{50}[a]**	**pK_b[a]**	**pEC_{50}[a]**	**pK_b[a]**
DMSO	7.41 ± 0.18	N.A.[b]	6.83 ± 0.27	N.A.[b]
1l	7.04 ± 0.05	4.08 ± 0.81	6.02 ± 0.50	5.45 ± 0.33
3a	7.49 ± 0.13	5.26 ± 0.16	7.23 ± 0.24	N.D.[c]
3c	7.25 ± 0.13	N.D.[c]	6.11 ± 0.69	5.27 ± 0.42
4b	7.36 ± 0.33	N.D.[c]	6.55 ± 0.36	N.D.[c]
4c	7.18 ± 0.25	N.D.[c]	6.45 ± 0.48	5.12 ± 0.20
5b	7.09 ± 0.11	4.49 ± 0.18	6.28 ± 0.20	5.45 ± 0.27

5c	7.64 ± 0.25	4.16 ± 0.48	6.91 ± 0.28	4.78 ± 0.18

[a]Values are reported as mean ± SEM and represent the mean of 3-6 experiments; pEC_{50} of individual replicates were used to calculate pK_b values, using the Schild equation; [b]N.A. = Not applicable. [c]N.D. = Not determined.

2.3. In Silico Characterization of Antagonist Binding to the A_1R and A_3R

To better understand the reduced affinity of the new derivatives compared to the lead compound **A**, molecular docking studies of **Compound A** and its chemical analogs, **1l, 3a, 3b, 4b, 4c, 5b, and 5c** were performed against the active and inactive A_1R and A_3R. Docking with the active structure was performed to take into consideration the high constitutive activity shown by the A_1R and A_3R [37,40]. Binding Free Energy (BFE) scores (Table S2, see Supporting Information) were calculated for each compound, which correlated with the experimentally determined binding affinities.

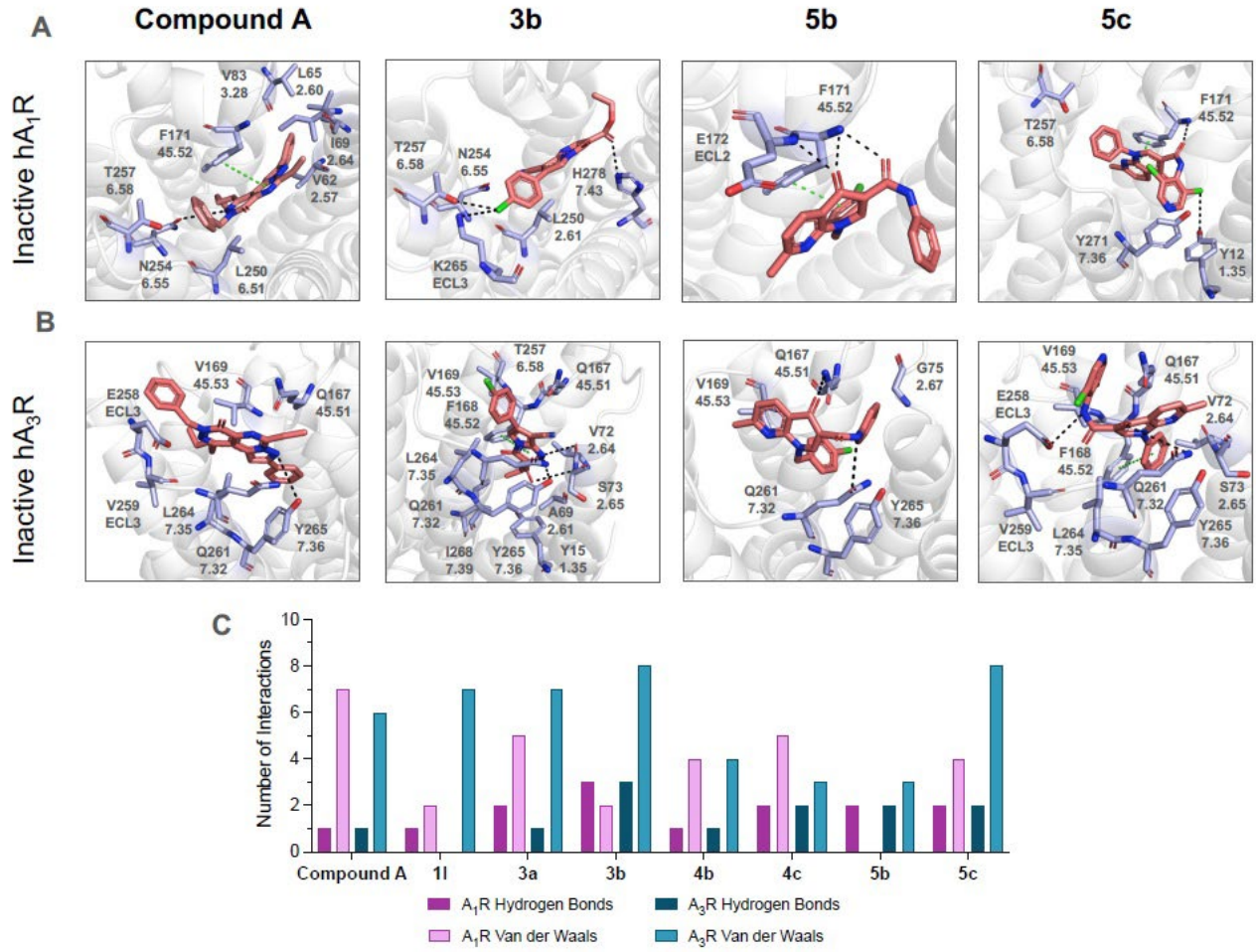

Figure 5. Predicted binding site of high affinity compounds, with number of interactions correlating with observed affinity. Docking at the inactive hA_1R (A) and hA_3R (B) of Compound **A**, **3b**, **5b**, **5c** (shown in orange). Interacting residues are highlighted in lilac, with hydrogen bonds

indicated by a black dashed line. Quantification of hydrogen bonds and van der Waals interactions (VDW) generated by each ligand's docking pose in the binding pocket (C).

To better understand the high affinity of **3b** and the other derivatives for both receptors, we looked at the predicted residues with which they interact, and summarized the predicted hydrogen bonds and Van der Waals interactions (**Figure 5A-B**, remaining compounds binding maps at the inactive ARs are found in Figure SF2 in Supporting Information). When bound to the inactive A_1R, **Compound A** tricyclic scaffold formed a π-π interactions with $F171^{45.52}$ and a stabilizing hydrogen bond with $N254^{6.55}$ (residue numbering as per [41,42]); both residues have been previously shown crucial for AR binding [38]. At the inactive A_3R, **Compound A** does not form π-π interactions with the equivalent $F168^{45.52}$, but instead makes an additional hydrogen bond with $Y265^{7.36}$ (**Figure 5A**). When bound to the inactive A_1R, **3b** formed an extensive hydrogen bond network; the phenyl chloride formed hydrogen bonds with $T257^{6.58}$ and K265 located in extracellular loop (ECL) 3, while its carbonyl group formed hydrogen bonds with $H278^{7.43}$. At the inactive A_3R, **3b** formed π-π interactions with $F168^{45.52}$. Hydrogen bonds were also formed between **3b**'s heterocyclic nitrogen and $V72^{2.64}$ and $Y265^{7.36}$, with **3b**'s carbonyl group forming a hydrogen bond with $S73^{2.65}$ (**Figure 5B**). Whilst **Compound A** formed the most interactions with the A_1R, **3b** and **5c** formed the most contacts with the A_3R.

The BFE scores for **5b** and **5c** showed the greatest difference when comparing the inactive and active ARs, with the experimentally observed A_3R selectivity (**Figure 2E, Figure 4D**) only apparent at the active structures (Table S2, see Supporting Information). However, when looking at the contact maps, both compounds displayed increased interactions with the A_3R compared to the A_1R (**Figure 5C**). When bound to the inactive A_1R, **5b** formed π-π interactions with $F171^{45.52}$ through its bicyclic scaffold. Its carbonyl groups formed hydrogen bonds with $E172^{ECL2}$, and phenyl group formed a π-stacking interaction with $F171^{45.52}$. **5c** when docked at the inactive A_1R, formed similar core π-π interactions with $F171^{45.52}$ through its bicyclic scaffold, with additional hydrogen bonds between its di-chloropyridine group and $Y12^{1.35}$ as well as its carbonyl group and $F171^{45.52}$. At the inactive A_3R, **5b** does not form π-π interactions with $F168^{45.52}$; it is instead stabilized via nonpolar interactions with

V169$^{45.53}$ and G75$^{2.67}$ and hydrogen bond formation with Q261$^{7.32}$. **5c** formed the same bicyclic scaffold π-π interactions with F168$^{45.52}$ at the inactive A_3R as in the A_1R. The di-chloropyridine nitrogen base linker formed hydrogen bonds with E258^{ECL3} while its carbonyl groups formed hydrogen bonds with and Q261$^{7.32}$ and additional polar interactions with Q167$^{45.51}$ (**Figure 5A and 5B**).

For further insight into the A_3R binding selectivity exhibited by **5b** and **5c**, Adaptive Poisson Boltzmann Solver (APBS) maps were generated alongside the docking poses at the inactive and active A_1R and A_3R. APBS is used to generate electrostatic potential maps that provide insight into the distribution of charged regions on the surface of biomolecules. These electrostatic mappings can be used to visualize and predict protein-ligand interaction sites and binding pose orientation [43]. Both inactive and active A_1R structures were determined to have the same charge gradients. However, whilst **5b** was able to identify the orthosteric pocket as its most energetically favorable binding pose for both structures, **5c** was only able to bind in the pocket at the inactive A_1R and not the active A_1R (**Figure 6A**). At the active and inactive A_3R, APBS mapping determined that the orthosteric pockets contained opposite charge gradients. However, when docked at either A_3R structure, both **5b** and **5c** were able to identify the orthosteric pocket for their energetically most favorable poses (**Figure 6B**).

Using the contact maps, it was predicted that a triad of polar residues (Q167$^{45.51}$, Q261$^{7.32}$, and E258^{ECL3}) contributed to these electrostatic interactions that stabilized **5b** and **5c** binding at the A_3R. Upon comparison, these were found not to be present in the A_1R, or the rat A_3R (rA_3R) (**Figure 6C**). We therefore used this naturally occurring variation to determine if these residues contribute to the difference in affinity. Neither **5b** nor **5c** was able to find the orthosteric pocket when docked against the human A_3R, mutated such that its binding pocket emulates the rA_3R. Both compounds showed a reduction in pK_b at the rA_3R when tested for their ability to antagonize **NECA** in a cAMP assay, confirming their reduced affinity at the rA_3R (**Figure 6D**).

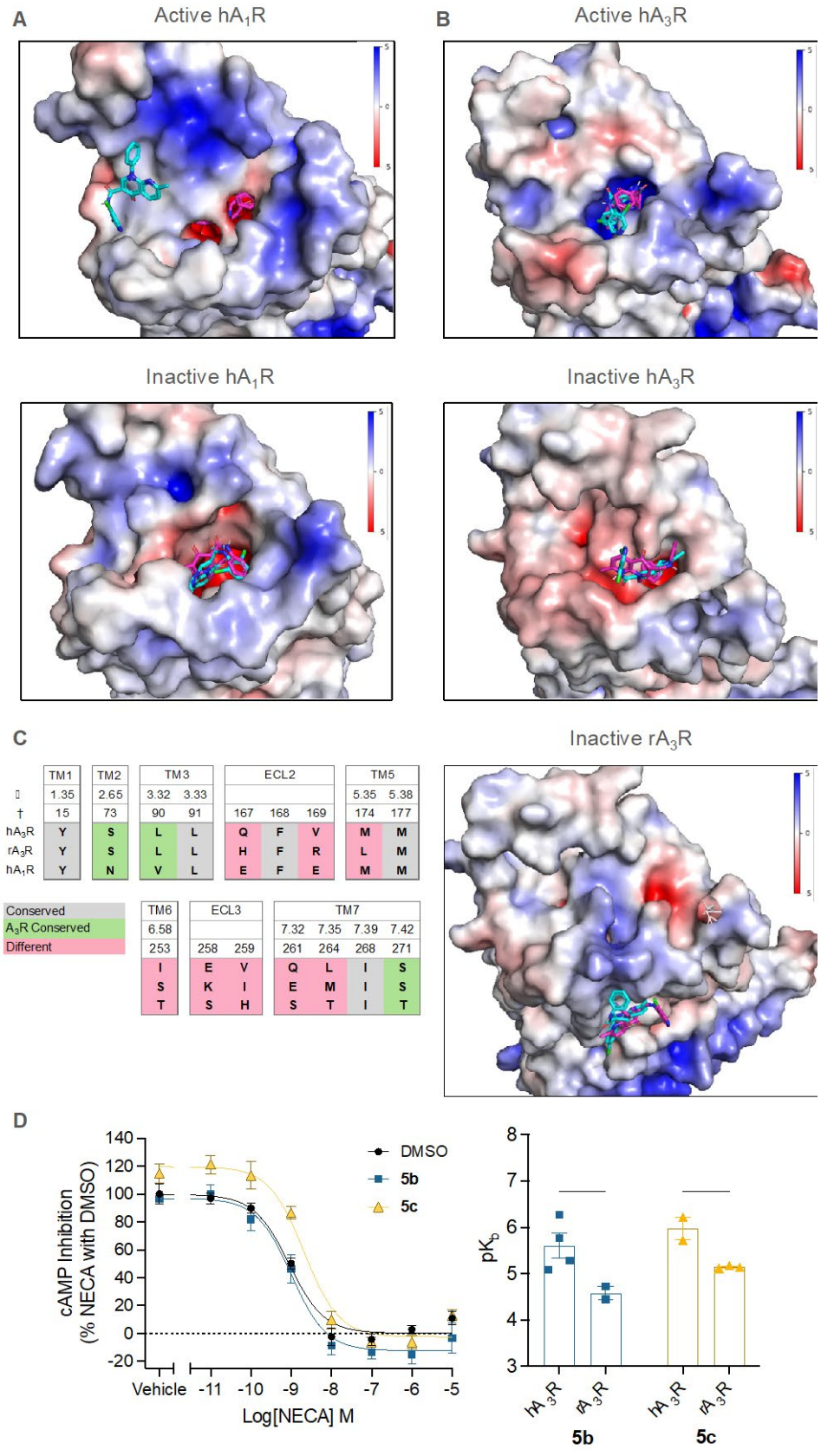

Figure 6. APBS integrated docking poses of 5b and 5c at the A1R, A3R, and ratA3R with pharmacology. Docking pose analysis of **5b** (pink) and **5c** (blue) at the active and inactive A_1R with A_1R (A). Docking pose analysis of **5b** and **5c** at the active and inactive A3R (B). hA_1R vs. hA_3R vs.

ratA$_3$R sequence map with docking at inactive ratA$_3$R (C). Pharmacology of **5b** and **5c** at the ratA$_3$R compared to the hA3R (D). Significant difference between hA$_3$R and rA$_3$R determined using a Two-Way ANOVA with Šidák's test for multiple comparisons * $p < 0.05$.

3. Conclusions

In this paper we have reported the development of a new series of A_1/A_3 adenosine receptor antagonists as simplification of pyrazolo[1′,5′:1,6]pyrimido[4,5-d]pyridazin-4(3H)-ones previously published by us. In particular, starting from the lead compound **A**, we synthesized 6/6- and 6/5-bicyclic compounds (pyrimido[4,5-d]pyridazine-4,8-diones, pyrazolo[1,5-a]pyrimidine-7-one, pyrrolo[1,2-a]pyrimidine, 1,8-naphtyridine and pyrido[1,2-a]pyrimidine) which were subjected to pharmacological studies to assess their binding affinity for the A_1R and A_3R using a NanoBRET competition binding assay. Computational experiments were conducted to gain further insight into the biophysical bases of the different selectivity features recorded through biological tests.

Pharmacological results highlighted that simplification to bicyclic scaffolds generally reduced both affinity and selectivity with respect to compound **A**, being the highest affinity values in the micromolar range. However, selectivity towards the A_3R was observed, suggesting a smaller scaffold is more suited to this subtype. Preliminary screening revealed a number of products with pKi ≥ 5 for A_1 or A_3 and as regard the scaffold, we can speculate that the 5/6-term cores (pyrazolo[1,5-a]pyrimidine and pyrazolo[1,5-a]pyrimidin-2-(1H)-one) are probably less suitable since out of nineteen compounds tested only three reached the pKi threshold, while the 6/6-term cores (both pyrimido[4,5-d]pyridazine and 1,8-naphthyridine, a total of 7 tested) provided four compounds active in the micromolar range. Overall, it is interesting to note that our working hypothesis (**Figure 1**) is largely confirmed by the biological results, since we find **1l** among the most interesting compounds. This ligand reflects in full the simplification of the lead **A** by formal elimination of the pyridazinone ring (structure **C**). In similar fashion, products **4b** and **4c** show scaffold **B** in the structure, as elimination of the pyrazole nucleus from lead **A**. Therefore, selected compounds showing a pKi ≥ 5 (**1l**, **3a**, **3b**, **4b**, **4c**, **5b** and **5c**) have been selected to define their binding profile and selectivity on A_{2A} and A_{2B}. From this study, compound **3b** emerged as the most potent A_1/A_3 mixed antagonist of

the series, with pKi = 6.41 and 6.29 for A_1R and A_3R respectively, while **5c** resulted the most selective term, with sub-micromolar affinity for the A_3R (pKi = 6.40) and 10-fold lower affinity for the other AR subtypes. These findings were supported by computational studies, with **3b** generating the most contacts amongst the analogue panel at the A_1R and A_3R (**Figure 5C**). The selectivity of **5c** was reaffirmed by only being able to identify an orthosteric pocket binding pose at the active A_3R and not the active A_1R (**Figure 6A**).

4. Experimental Section

4.1. General remarks

All melting points were determined on a Bűchi instrument (New Castle, DE) and are uncorrected. Extracts were dried over Na_2SO_4, and the solvents were removed under reduced pressure. Merck F-254 commercial plates (Merck, Durham, NC) were used for analytical TLC to follow the course of the reactions. Silica gel 60 (Merck 70-230 mesh, Merck, Durham, NC) was used for column chromatography. Nomenclatures follow the IUPAC naming system. ^1H and ^{13}C NMR spectra were recorded using an internal deuterium lock at ambient probe temperatures on a Bruker DRX-400 (400 MHz) instrument and using a sample prepared by dissolving 5 mg of the complex in ca. 500 μL of DMSO-d_6. Chemical shifts (δ) are quoted in ppm, to the nearest 0.01 ppm (for ^1H NMRs), or 0.01 ppm (for ^{13}C NMRs), and are referenced to the residual non-deuterated solvent peak. Coupling constants (J) are reported in hertz (Hz) to the nearest 0.1 Hz. Data are reported as follows: chemical shift, multiplicity (br = broad; s = singlet; d = doublet; t = triplet; m = multiplet, or as a combination of these, i.e., dd, dt, etc.), integration, coupling constant(s) and assignment . Assignments were determined either based on unambiguous chemical shift or coupling pattern, supported by DEPT) or by analogy to fully interpreted spectra for related compounds. For analytical HPLC, a XTerra RP18 (5 μm, 4.6 mm × 100 mm) column was used and the mobile phase was composed of solvent A (99.9% water, 0.1% trifluoroacetic acid) and solvent B (99.9% acetonitrile, 0.1% trifluoroacetic acid) used in a linear gradient (4% B for 6min, increasing from 4% B to 90% B for 20 min, decreasing from 90%

B to 4% B for 7 min, 4% B for 5min, total run time = 38 min). The sample solutions were prepared at a concentration of 0.05-0.1 mg per 1 mL. The injection volume was 50 µL, the flow rate was 0.3 mL min^{-1}. The column temperature was room temperature. The UV detector wavelength was fixed at 250nm. The values of retention time (t_R) are given in minutes. High resolution mass spectrometry (HR-MS) analyses, for accurate mass determination, were performed on Waters Xevo G2-XS (operating in ES^+ or ES^- mode) through direct infusion of samples at 5 µL/min. Unless otherwise mentioned, electron spray ionisation (ESI) conditions were as follows: 3 kV (ES) capillary voltage; 70 V (ES) sample cone voltage; 250 °C desolvation temperature; 120 °C source temperature.

4.2. Chemistry

6-Ethyl-2-phenylpyrazolo[1,5-a]pyrimidin-7(4H)-one (1a). A solution of commercially available **6** (1.0 mmol) and ethyl formylbutanoate (1.0 mmol) in ethanol, containing a catalytic amount of acetic acid, was refluxed for 10-30 minutes. After cooling, the precipitate was filtered off and washed with ethanol/water and recrystallized from acetic acid. Yield 68%, mp > 300; ^{1}H NMR (400 MHz, DMSO-d_6) δ 12.07 (brs, 1H, NH), 8.21 (s, 1H, Ar), 7.69 (s, 1H, Ar), 7.59 (d, 2H, J = 6.7 Hz, Ar), 7.46 (t, 2H, J = 7.7 Hz, Ar), 7.29 (t, 1H, J = 7.4 Hz, Ar), 2.47 (q, 2H, J = 7.4 Hz, CH_2), 1.15 (t, 3H, J = 7.4 Hz, CH_3). ^{13}C NMR (100 MHz, DMSO-d_6) δ 156.97 (C), 141.80 (CH), 137.50 (C), 136.08 (CH), 130.81 (C), 128.91 (2×CH), 126.48 (2×CH), 126.25 (CH), 110.25 (C), 103.66 (C), 20.10 (CH_2), 13.88 (CH_3). HR-MS(ESI): calcd for $C_{14}H_{13}N_3O$ 239.1059 (m/z), found m/z 240.1156 $[M + H]^+$, m/z 262.0988 $[M + Na]^+$, m/z 278.0706 $[M + K]^+$. t_R= 26.449 min.

Ethyl 7-oxo-2-phenyl-4,7-dihydropyrazolo[1,5-a] pyrimidine-6-carboxylate (1b)[29]. ^{1}H NMR (400 MHz, DMSO-d_6) 8.57 (s, 1H, Ar), 7.99 (d , 2H, J = 8.0 Hz, Ar), 7.51-7.43 (m, 3H, Ar), 6.79 (s, 1H, Ar), 4.25 (q, 2H, J = 7.1 Hz, CH_2), 1.30 (t, 3H, J = 7.1 Hz, CH_3). ^{13}C NMR (100 MHz, DMSO-d_6) δ 163.50 (C), 153.59 (C), 145.16 (CH), 141.65 (C), 139.56 (C), 132.00 (C), 129.27 (CH), 128.81 (2×CH), 126.23 (2×CH), 98.97 (C), 88.37 (CH), 59.98 (CH_2), 14.28 (CH_3). HR-MS(ESI): calcd for $C_{15}H_{13}N_3O_3$ 283.0957 (m/z), found m/z 306.0866 $[M + Na]^+$. t_R= 25.564 min.

Ethyl 4-methyl-7-oxo-2-phenyl-4,7-dihydropyrazolo[1,5-a]pyrimidine-6-carboxylate (1c). Methyl iodide (2.0 mmol) was added to a mixture of compound **1b** [29] (1.0 mmol) and K_2CO_3 (1.0 mmol) in anhydrous DMF (5 mL). The reaction was maintained at 40 °C for two hours, monitoring by TLC (dichloromethane/methanol 10/1, v/v). After complete consumption of the starting material, dilution with water/ice gave a white precipitate which was filtered off and recrystallized from ethanol. Yield 52 %, mp 254-256 °C; ^{1}H NMR (400 MHz, DMSO-d_6) δ 8.66 (s, 1H, Ar), 7.98 (d, 2H, J = 8.0 Hz, Ar), 7.53-7.42 (m, 3H, Ar), 7.05 (s, 1H, Ar), 4.25 (q, 2H, J = 7.1 Hz, CH_2), 3.85 (s, 3H, NCH_3), 1.29 (t, 3H, J = 7.1 Hz, CH_3). ^{13}C NMR (100 MHz, DMSO-d_6) δ 163.43 (C), 154.47 (CH), 153.51 (C), 149.04 (CH), 143.61 (C), 131.86 (C), 129.34 (CH), 128.96 (2×CH), 126.17 (2×CH), 99.09 (C), 89.19 (CH), 60.13 (CH_2), 40.46 (CH_3), 14.33 (CH_3). HR-MS(ESI): calcd for $C_{16}H_{15}N_3O_3$ 297.1113 (m/z), found m/z 298.3531 $[M + H]^+$, 320.1006 $[M + Na]^+$, m/z 336.0735 $[M + K]^+$. t_R= 26.356 min.

General procedure for the synthesis of compounds 1d and 1e. A solution of compound **1b** or **8** [29] (2.0 mmol) suspended in glacial acetic acid (15 mL) was heated to facilitate the solubilization. Subsequently, a sulphonitric mixture (HNO_3/H_2SO_4, 3:0.5 mL) was slowly added under stirring. The orange precipitate was cooled and poured into water/ice, obtaining a light-yellow residue which was filtered off, washed twice with water and then purified by recrystallization from the suitable solvent.

Ethyl 3-nitro-7-oxo-2-phenyl-4,7-dihydropyrazolo[1,5-a]pyrimidine-6-carboxylate (1d)

From **1b** [29]; recrystallized from ethanol. Yield 70 %, mp 296-297 °C; ^{1}H NMR (400 MHz, DMSO-d_6) δ 8.42 (s, 1H, Ar), 7.73 (d, 2H, J = 8.0 Hz, Ar), 7.54 (d, 3H, J = 8.0 Hz, Ar), 4.29 (q, 2H, CH_2, J = 7.1 Hz), 1.31 (t, 3H, CH_3, J = 7.1 Hz). ^{13}C NMR (100 MHz, DMSO) δ 162.37 (C), 151.49 (C), 149.27 (C), 146.09 (CH), 140.72 (C), 130.03 (C), 129.60 (CH), 129.53 (2×CH), 128.17 (2×CH), 117.57 (C), 104.64 (C), 60.82 (CH_2), 14.17 (CH_3). HR-MS(ESI): calcd for $C_{15}H_{12}N_4O_5$ 328.0808 (m/z), found m/z 329.0859 $[M + Na]^+$, 351.0686 $[M + Na]^+$, m/z 367.0430 $[M + K]^+$. t_R= 27.105 min.

4-Methyl-3-nitro-2-phenylpyrazolo[1,5-a]pyrimidin-7(4H)-one (1e)

From **8** (2.5 mmol) [29]; recrystallized fom ethanol. Yield 65 %, mp > 300 °C; ^{1}H NMR (400 MHz, DMF-d_7 + CH_2Cl_2) δ 9.60 (s, 1H, Ar), 8.45-8.37 (m, 5H, Ar), 7.56 (s, 1H, Ar), 4.18 (s, 3H, CH_3). ^{13}C NMR (100 MHz, DMF-d_7 + CH_2Cl_2) δ 152.89 (C), 148.72 (C), 147.37 (C), 147.09 (CH), 143.90 (C), 138.23 (C), 127.48 (2×CH), 124.36 (2×CH), 91.86 (CH), 41.12 (CH_3). HR-MS(ESI): calcd for $C_{13}H_{10}N_4O_3$ 270.0753 (m/z), found m/z 293.2022 $[M + Na]^+$. t^R= 26.706 min.

General procedure for the synthesis of 1f and 1g. NBS (1.5 mmol) was added to a solution of compound **1b** [29] or **7** (for the synthesis of **7** see below) (1.0 mmol) in dichloromethane (10 mL). The brown solution was maintained at room temperature for 1 hour and then evaporated to dryness. The residue was washed with alkaline water, before being recovered by filtration and recrystallized from the suitable solvent.

Ethyl 3-bromo-7-oxo-2-phenyl-4,7-dihydropyrazolo[1,5-a]pyrimidine-6-carboxylate (1f)

From **1b** [29]; recrystallized from acetonitrile. Yield 68 %, mp 266-267 °C; ^{1}H NMR (400 MHz, DMSO-d_6) δ 8.42 (s, 1H, Ar), 7.93 (d, 2H, J = 8.0 Hz, Ar), 7.57-7.47 (m, 3H, Ar), 4.25 (q, 2H, J = 7.1 Hz, CH_2), 1.30 (t, 3H, J = 7.1 Hz, CH_3). ^{13}C NMR (100 MHz, DMSO-d_6) δ 163.23 (C), 152.37 (C), 150.63 (C), 145.54 (CH), 140.18 (C), 130.93 (C), 129.43 (CH), 128.69 (2×CH), 127.84 (2×CH), 99.89 (C), 75.50 (C), 60.22 (CH_2), 14.25 (CH_3). HR-MS(ESI): calcd for $C_{15}H_{12}BrN_3O_3$ 361.0062 (m/z), found m/z 383.9940, 385.9921 $[M + Na]^+$, m/z 399.9680, 401.9659 $[M + K]^+$. t_R= 26.356 min.

3-Bromo-5,6-dimethyl-2-phenylpyrazolo[1,5-a]pyrimidin-7(4H)-one (1g)

From **7**; recrystallized from acetonitrile. Yield 68 %, mp 233-235 °C; ^{1}H NMR (400 MHz, DMSO-d_6) δ 12.07 (exch br s, 1H, NH), 7.92 (d, 2H, J = 8.0 Hz, Ar), 7.54-7.46 (m, 3H, Ar), 2.38 (s, 3H, CH_3), 1.99 (s, 3H, CH_3). ^{13}C NMR (100 MHz, DMSO-d_6) δ 156.12 (C), 149.83 (C), 146.97 (C), 140.09 (C), 131.44 (C), 129.08 (CH), 128.52 (2×CH), 127.83 (2×CH), 126.11 (C), 102.17 (CH), 71.19 (C), 17.10 (CH_3), 10.42 (CH_3). HR-MS(ESI): calcd for $C_{14}H_{12}BrN_3O$ 317.0164 (m/z), found m/z 318.0239, 320.0222 $[M + H]^+$, m/z 340.0064, 342.0042 $[M + Na]^+$, m/z 355.9800, 357.9779 $[M + K]^+$. t_R= 27.882 min.

3,6-Dibromo-5-methyl-2-phenylpyrazolo[1,5-a]pyrimidin-7(4H)-one (1h)

Compound **9** (2.5 mmol) [34] was suspended in hot acetic acid (10 mL) and an excess of bromine was added until the solution remained red. The dilution of the solution with ice/water yielded a precipitate which was filtered and purified by recrystallization from DMF/water. Yield 52%, mp 251-253 °C; ^{1}H NMR (400 MHz, DMSO-d_6) δ 12.83 (exch br s, 1H, NH), 7.931 (d, 2H, J = 8.0 Hz, Ar), 7.56-7.48 (m, 3H, Ar), 2.55 (s, 3H, CH_3). ^{13}C NMR (100 MHz, DMSO-d_6) δ 152.34 (C), 150.62 (C), 150.09 (C), 139.89 (C), 131.05 (C), 129.35 (CH), 128.63 (2×CH), 127.91 (2×CH), 92.96 (C), 72.85 (C), 20.52 (CH_3). HR-MS(ESI): calcd for $C_{13}H_9Br_2N_3O$ 380.9112 (m/z), found m/z 381.9183, 383.9162, 385.9143 $[M + H]^+$, 403.9004, 405.8985, 407.8964 $[M + Na]^+$, m/z 419.8742 421.8722, 423.8702 $[M + K]^+$. t_R= 29.089 min.

General procedure for obtaining compounds 1i and 1j. Starting esters **1d** and **1f** were suspended in a NaOH 20% solution and heated until complete solubilization. After cooling, the addition of HCl conc. gave the precipitate of the corresponding carboxylic acids **1i** and **1j**, which were recovered by vacuum filtration.

3-Nitro-7-oxo-2-phenyl-4,7-dihydropyrazolo[1,5-a]pyrimidine-6-carboxylic acid (1i)

From **1d**; yield 80 %, mp 253-254 °C; ^{1}H NMR (400 MHz, DMSO-d_6) δ 8.46 (s, 1H, Ar), 7.73 (d, 2H, J = 8.0 Hz, Ar), 7.55-750 (m, 3H, Ar). ^{13}C NMR (100 MHz, DMSO-d_6) δ 163.86 (C), 152.87 (C), 149.50 (CH), 146.92 (C), 141.37 (C), 129.98 (C), 129.75 (CH), 129.53 (2×CH), 128.15 (2×CH), 117.68 (C), 104.55 (C). HR-MS(ESI): calcd for $C_{13}H_8N_4O_5$ 300.0495 (m/z), found m/z 323.0370 $[M + Na]^+$. t_R= 25.341 min.

3-Bromo-7-oxo-2-phenyl-4,7-dihydropyrazolo[1,5-a]pyrimidine-6-carboxylic acid (1j)

From **1f**; yield 83 %, mp 253-254 °C; ^{1}H NMR (400 MHz, DMSO-d_6) δ 8.49 (s, 1H, Ar), 7.94 (d, 2H, J = 8.0 Hz, Ar), 7.57-7.51 (m, 3H, Ar). ^{13}C NMR (100 MHz, DMSO-d_6) δ 164.64 (C), 155.41 (C), 151.16 (C), 146.39 (CH), 141.23 (C), 130.92 (C), 129.47 (CH), 128.68 (2×CH), 127.87 (2×CH), 99.22 (C), 76.30 (C). HR-MS(ESI): calcd for $C_{13}H_8BrN_3O_3$ 332.9749, (m/z), found m/z 355.9622, 357.9600 $[M + Na]^+$. t_R= 26.582 min.

3-Benzylideneamino-5-methyl-2-phenylpyrazolo[1,5-a]pyrimidin-7(4H)-one (1k)

A suspension of **11** (2.0 mmol) (for the synthesis of **11** see below) and benzaldehyde (2.2 mmol) was refluxed in ethanol (20 mL) for 10 min. The yellow precipitate was filtered and recrystallized from acetic acid. Yield 75%, mp 299-301 °C; ^{1}H NMR (400 MHz, DMSO-d_6) δ 12.09 (exch br s, 1H, NH), 8.71 (s, 1H, Ar), 8.03 (d, 2H, *J* = 8.0 Hz, Ar), 7.92 (d, 2H, *J* = 8.0 Hz, Ar), 7.55-7.38 (m, 6H, Ar), 5.67 (s, 1H, Ar), 2.35 (s, 3H, CH_3). ^{13}C NMR (100 MHz, DMSO-d_6) δ 161.74 (CH), 155.74 (C), 150.98 (C), 146.53 (C), 136.48 (C), 132.59 (C), 132.48 (C), 131.13 (CH), 128.78 (2×CH), 128.56 (CH), 128.46 (2×CH), 128.21 (2×CH), 127.80 (2×CH), 115.22 (C), 95.91 (CH), 18.84 (CH_3). HR-MS(ESI): calcd for $C_{20}H_{16}N_4O$ 328.1324 (m/z), found m/z 329.1394 $[M + H]^+$, m/z 351.1250 $[M + Na]^+$. t_R= 23.763 min.

6-Cyano-3-phenylpyrazolo[1,5-a]pyrimidin-7(4H)-one (1l)

A solution of commercially available 4-phenyl-5(3)-aminopyrazole **12** (1.0 mmol), ethyl alpha-formylcyanoacetate **13** (1.0 mmol) and glacial acetic acid (catalytic amount) in ethanol (5 mL) was refluxed for 30 minutes. After cooling, the precipitate was recovered by filtration, washed with ethanol/water and recrystallized from a suitable solvent. Yield 70%, mp > 300 °C, ^{1}H NMR (400 MHz, DMSO-d_6) δ 8.65 (s, 1H, Ar), 8.35 (s, 1H, Ar), 7.61 (d, 2H, *J* = 8.0 Hz, Ar), 7.47 (t, 2H, J = 8.0 Hz, Ar), 7.35 (t, 1H, *J* = 8.0 Hz, Ar). ^{13}C NMR (100 MHz, DMSO-d_6) δ 154.60 (C), 147.85 (CH), 143.01 (CH), 137.07 (C), 129.61 (C), 128.88 (2×CH), 127.36 (2×CH), 127.17 (CH), 115.56 (C), 107.81 (C), 82.88 (C). HR-MS(ESI): calcd for $C_{13}H_8N_4O$ 236.0698 (m/z), found m/z 237.0784 $[M + H]^+$, 259.0623 $[M + Na]^+$. t_R= 25.199 min.

6-Methyl-2-phenylpyrazolo[1,5-a] pyrimidin-7(4H)-one (1m) [30]**.** ^{1}H NMR (400 MHz, DMSO-d_6) δ 12.23 (exch br s, 1H, NH), 7.97 (d, 2H, *J* = 8.0 Hz, Ar), 7.81 (d, 1H, *J* = 4.6 Hz, Ar), 7.48-7.38 (m, 3H, Ar), 6.57 (s, 1H, Ar), 2.01 (s, 3H, CH_3). ^{13}C NMR (100 MHz, DMSO-d_6) δ 157.45 (C), 153.08 (C), 143.01 (C), 136.19 (CH), 132.55 (C), 128.83 (CH), 128.71 (2×CH), 126.17 (2×CH), 103.64 (C), 85.13 (CH), 12.64 (CH_3). HR-MS(ESI): calcd for $C_{13}H_{11}N_3O$ 225.0902 (m/z), found m/z 226.0984 $[M + H]^+$, m/z 248.0805 $[M + Na]^+$, m/z 264.0542 $[M + K]^+$. t_R= 25.193 min.

4-Methyl-7-oxo-2-phenyl-4,7-dihydropyrazolo[1,5-a] pyrimidine-5-carboxylic acid (1n) [30]**.**

^{1}H NMR (400 MHz, DMSO-d_6) δ 8.00 (d, 2H, J = 8.0 Hz, Ar), 7.52-7.42 (m, 3H, Ar), 7.07 (s, 1H, Ar), 6.21 (s, 1H, Ar), 3.85 (s, 3H, NCH_3). ^{13}C NMR (100 MHz, DMSO-d_6) δ 162.83 (C), 155.23 (C), 153.82 (C), 145.29 (C), 143.56 (C), 131.94 (C), 129.30 (CH), 128.88 (2×CH), 126.17 (2×CH), 98.77 (CH), 88.45 (CH), 38.04 (CH_3). HR-MS(ESI): calcd for $C_{14}H_{11}N_3O_3$ 269.0800 (m/z), found m/z 270.0886 $[M + H]^+$, 284.1050 $[M(+CH_3) + H]^+$ m/z 292.0702 $[M + Na]^+$. t_R= 22.747 min.

6-Acetyl-7-methyl-3-phenylpyrazolo[1,5-a]pyrimidin-2(1H)-one (2a)

A solution of commercially available 5-amino-4-phenylpyrazolo-3-one **14** (50 mmol) in 2N HCl/ethanol (25 mL/15 mL) was heated at 60 °C. The addition of 8 mL (52.2 mmol) of ethoxymethylenacetylacetone produced the simultaneous formation of an orange precipitate and the suspension was heated at the same temperature for additional 30 minutes. After cooling, the suspension was neutralized with 2N NaOH (25 mL). The precipitate was recovered by filtration and recrystallized from ethanol, affording light yellow crystals. Yield 60 %, mp 203-204 °C, TLC eluent: chloroform/methanol 10/1 v/v. ^{1}H NMR (400 MHz, DMSO-d_6) δ 8.92 (s, 1H, Ar), 8.23 (d, 2H, J = 8.0 Hz, Ar), 7.40 (t, 2H, J = 8.0 Hz, Ar), 7.20 (t, 1H, J = 8.0 Hz, Ar), 2.94 (s, 3H, CH_3), 2.64 (s, 3H, CH_3). ^{13}C NMR (100 MHz, DMSO-d_6) δ 196.58 (C), 166.36 (C), 149.78 (CH), 144.90 (C), 138.64 (C), 131.93 (C), 128.12 (2×CH), 126.23 (2×CH), 125.22 (CH), 116.28 (C), 93.69 (C), 29.58 (CH_3), 15.00 (CH_3). HR-MS(ESI): calcd for $C_{15}H_{13}N_3O_2$ 267.1008 (m/z), found m/z 268.1091 $[M + H]^+$. t_R= 28.934 min.

6-Acetyl-3-bromo-7-methylpyrazolo[1,5-a]pyrimidin-2(1H)-one (2b) [31]. ^{1}H NMR (400 MHz, DMSO-d_6) δ 12.31 (exch br s, 1H, NH), 8.91 (s, 1H, Ar), 2.91 (s, 3H, CH_3), 2.64 (s, 3H, CH_3). ^{13}C NMR (100 MHz, DMSO-d_6) δ 196.69 (C), 164.28 (C), 150.81 (CH), 149.20 (C), 145.18 (C), 117.13 (C), 69.56 (C), 29.72 (CH_3), 14.49 (CH_3). HR-MS(ESI): calcd for $C_9H_8BrN_3O_2$ 268.9800 (m/z), found m/z 269.9882, 271.9866 $[M + H]^+$. t_R= 24.375 min.

6-Acetyl-3-bromo-1,7-dimethylpyrazolo[1,5-a]pyrimidin-2(1H)-one (2c)

K_2CO_3 (1.0 mmol) and methyl iodide (2.0 mmol) were added to a solution of compound **2b** [31] (1.0 mmol) in 5 mL of anhydrous DMF. The reaction was maintained at 50 °C for 2 hours, monitoring by

TLC (dichloromethane/methanol 10/1, v/v). After full consumption of the starting material, the mixture was diluted with water/ice, to give a light-yellow precipitate which was recovered by filtration and recrystallized from ethanol. Yield 67 %, mp 171-172 °C; ^{1}H NMR (400 MHz, DMSO-d_6) δ 8.97 (s, 1H, Ar), 4.09 (s, 3H, NCH_3), 2.96 (s, 3H, CH_3), 2.65 (s, 3H, CH_3). ^{13}C NMR (100 MHz, DMSO-d_6) δ 196.63 (C), 164.46 (C), 151.60 (CH), 150.07 (C), 145.42 (C), 117.35 (C), 69.23 (C), 56.61 (CH_3), 29.77 (CH_3), 14.50 (CH_3). HR-MS(ESI): calcd for $C_{14}H_{13}N_3O$ 282.9956 (m/z), found m/z 284.0050, 286.0024 $[M + H]^+$. t_R= 29.006 min.

Ethyl 7-(4-chlorophenyl)-8-cyano-4-thioxo-1,4-dihydropyrrolo[1,2-a]pyrimidine-3-carboxylate (3a)

0.72 mmol of Lawesson's reagent were added to a suspension of compound **15** (0.36 mmol) and ethyl 7-(4-chlorophenyl)-8-cyano-4-oxo-1,4-dihydropyrrolo[1,2-a]pyrimidine-3-carboxylate [32] in 5 mL of anhydrous toluene. The mixture was stirred at reflux for 6 h and then cooled, concentrated in vacuo, diluted with ice-cold water (10 mL) and extracted with ethyl acetate (3 x 15 mL). The organic phase was dried over sodium sulphate and evaporated under vacuum to obtain the final compound **3a** which was purified by flash column chromatography using cyclohexane/ethyl acetate 3:1 as eluent. Yield 70%, mp > 300 °C, ^{1}H NMR (400 MHz, DMSO-d_6) δ 8.31 (s, 1H, Ar), 8.28 (s, 1H, Ar), 7.78 (d, 2H, J = 8.0 Hz, Ar), 7.53-7.40 (m, 3H, Ar), 4.26 (q, 2H, J = 7.1 Hz, CH_2), 1.31 (t, 3H, J = 7.1 Hz, CH_3). ^{13}C NMR (100 MHz, DMSO) δ 173.23 (C), 164.65 (C), 138.55 (CH), 136.93 (C), 131.58 (C), 129.12 (2×CH), 128.40 (CH), 126.84 (2×CH), 115.06 (C), 114.47 (C), 111.16 (CH), 75.57 (C), 60.57 (CH_2), 14.11 (CH_3). HR-MS(ESI): calcd for $C_{17}H_{13}N_3O_2S$ 323.0728 (m/z), found m/z 324.0869 $[M + H]^+$, m/z 346.0679 $[M + Na]^+$. t_R= 31.024 min.

Ethyl 8-cyano-4-oxo-7-phenyl-1,4-dihydropyrrolo[1,2-a] pyrimidine-3-carboxylate (3b) [32]**.** ^{1}H NMR (400 MHz, DMSO-d_6) δ 8.40 (s, 1H, Ar), 7.78 (d, 2H, J = 8.0 Hz, Ar), 7.71 (s, 1H, Ar), 7.57-7.52 (m, 2H, Ar), 4.21 (q, 2H, J = 7.1 Hz, CH_2), 1.28 (t, 3H, J = 7.1 Hz, CH_3). ^{13}C NMR (100 MHz, DMSO-d_6) δ 164.41 (C), 154.03 (C), 148.93 (C), 139.85 (C), 132.41 (C), 131.22 (CH), 128.97 (2×CH), 128.28 (2×CH), 125.63 (C), 115.95 (C), 107.01 (CH), 96.91 (C), 75.38 (C), 59.49 (CH_2),

14.38 (CH_3). HR-MS(ESI): calcd for $C_{17}H_{12}ClN_3O_3$ 341.0567 (m/z), found m/z 364.0529, 366.0498 $[M + Na]^+$. t_R= 30.468 min

7-Ethyl-5-phenyl-3,7-dihydropyrimido[4,5-d] pyridazine-4,8-dione (4a) [33]**.** ^1H NMR (400 MHz, DMSO-d_6) δ 13.07 (exch br s, 1H, NH), 8.43 (s, 1H, Ar), 7.42-7.34 (m, 5H, Ar), 4.17 (q, 2H, J = 7.1 Hz, CH_2), 1.30 (t, 3H, J = 7.1 Hz, CH_3). ^{13}C NMR (100 MHz, DMSO-d_6) δ 151.99 (CH), 144.19 (C), 136.66 (2 x C), 128.91 (2 x CH), 128.05 (CH), 127.14 (2 x CH), 46.65 (CH_2), 13.21 (CH_3). HR-MS(ESI): calcd for $C_{14}H_{12}N_4O_2$ 268.0960 (m/z), found m/z 269.1036 $[M + H]^+$, 291.0856 $[M + Na]^+$. t_R= 23.365 min.

5-(3-Chlorophenyl)-7-(cyclopentylmethyl)-3,7-dihydropyrimido[4,5-d]pyridazine-4,8-dione (4b). A mixture of **17b** (for the synthesis of **17b** see below) (0.58 mmol), triethylorthoformate (8.9 mmol, 1.5 mL) and a catalytic amount of concentrated sulfuric acid (0.05 mmol) was heated at 130 °C for 1 h in a sealed tube. After cooling, the precipitate was recovered by filtration under vacuum. The crude precipitate was purified by flash column chromatography using CH_2Cl_2/MeOH 9:1 as eluent. Yield 44%, mp = 266-268 °C (EtOH). ^1H NMR (400 MHz, DMSO-d_6) δ 8.45 (s, 1H, Ar), 7.47-7.36 (m, 4H, Ar), 4.09 (d, 2H, J = 7.5 Hz, N-CH_2), 2.46-2.38 (quin, 1H, J = 7.5 Hz, CH cC_5H_9), 1.63-1.49 (m, 6H, 3 x CH_2 cC_5H_9), 134-128 (m, 2H, CH_2 cC_5H_9.) ^{13}C NMR (100 MHz, DMSO-d_6) δ 158.17 (C), 156.84 (C), 152.05 (C), 149.88 (C), 148.52 (C), 142.31 (C), 138.69 (C), 131.77 (CH), 129.10 (CH), 128.79 (CH), 127.99 (CH), 127.63 (CH), 55.52 (CH_2), 38.54 (CH), 29.56 (CH_2), 24.47 (CH_2). HR-MS(ESI): calcd for $C_{18}H_{17}ClN_4O_2$ 356.1040 (m/z), found m/z m/z 379.0936, 381.0911 $[M + Na]^+$. t_R= 29.870 min.

5-(3-Chlorophenyl)-7-cyclohexyl-3,7-dihydropyrimido[4,5-d]pyridazine-4,8-dione (4c) [33]**.** ^1H NMR (400 MHz, DMSO-d_6) δ 8.44 (s, 1H, Ar), 7.48-7.38 (m, 4H, Ar), 4.84 (t, 1H, J = 7.0 Hz, CH cC_6H_{11}), 1.83-1.63 (m, 7H, cC_6H_{11}), 1.46-1.36 (m, 2H, cC_6H_{11}), 1.21-1.12 (m, 1H, cC_6H_{11}). ^{13}C NMR (100 MHz, DMSO-d_6) δ 158.09 (C), 156.30 (C), 151.90 (CH), 148.28 (C), 142.12 (C), 138.87 (C), 131.78 (C), 129.11 (CH), 128.83 (CH), 127.97 (CH), 127.66 (CH), 118.45 (C), 56.71 (CH), 30.56

(2×CH_2), 24.97 (2×CH_2), 24.84 (CH_2). HR-MS(ESI): calcd for $C_{18}H_{17}ClN_4O_2$ 356.1040 (m/z), found m/z 357.1117, 359.1110 $[M + H]^+$, 379.0944, 381.0919 $[M + Na]^+$. t_R= 29.599 min.

Ethyl 1-(3-fluorobenzyl)-7-methyl-4-oxo-1,4-dihydro-1,8-naphthyridine-3-carboxylate (5a). Compound **5a** was obtained following the same procedure for the synthesis of **17b**, but starting from intermediate **18** [33] and using *m*-F-benzyl bromide as reagent. The crude compound was purified by flash column chromatpgraphy using toluene/ethyl acetate 1:1 as eleunt. Yield 80%, mp = 139-141 °C (cyclohexane). ^{1}H NMR (400 MHz, DMSO-d_6) δ 8.98 (s, 1H, Ar), 8.44 (d, 1H, *J* = 8.1 Hz, Ar), 7.47-7.40 (m, 3H, Ar), 7.16 (t, 2H, *J* = 8.0 Hz, Ar), 5.66 (s, 2H, N-CH_2), 4.24 (q, 2H, *J* = 7.1 Hz, O-CH_2), 2.61 (s, 3H, CH_3), 1.28 (t, 3H, *J* = 7.1 Hz, CH_2CH_3) . ^{13}C NMR (100 MHz, DMSO-d_6) δ 173.18 (C), 164.28 (C), 162.44 (C), 160.40 (C), 149.26 (CH), 148.36 (C), 136.08 (CH), 133.04 (C), 130.11 (C), 130.03 (CH), 121.35 (CH), 120.56 (C), 115.51 (CH), 115.29 (CH), 111.75 (C), 59.96 (CH_2), 51.79 (CH_2), 24.56 (CH_3), 14.26 (CH_3). HR-MS(ESI): calcd for $C_{19}H_{17}FN_2O_3$ 340.1223 (m/z), found m/z 341.1312 $[M + H]^+$, 363.1184 $[M + Na]^+$, m/z 379.0880 $[M + K]^+$. t_R= 29.533 min.

General procedure for the synthesis of the final compounds 5b and 5d. The appropriate carboxylic acid **20a** or **21** [33] (0.24 mmol) was converted into the acyl chloride with $SOCl_2$ (6.5 mmol) and triethylamine (0.06 mL) at room temperature for 40–60 min. After removing the excess $SOCl_2$, the residue was washed 3 times with cyclohexane and used in the following step without further purification. Under stirring at 0 °C, a solution of the obtained acyl chloride in anhydrous THF (5-7 mL) was added dropwise to a solution of the appropriate amine (2.6 mmol) in anhydrous THF (3-7 mL). The mixture was stirred at room temperature for 2-3 h. After removal of the solvent, the residue was treated with cold water and extracted with CH_2Cl_2 (3 × 15 mL). The crude amides **5b,d** were purified by flash column chromatography using toluene/ethyl acetate 10:1 (for **5b**) or CH_2Cl_2/MeOH 20:1 (for **5d**) as eluents.

1-(4-Chlorobenzyl)-7-methyl-4-oxo-N-phenyl-1,4-dihydro-1,8-naphthyridine-3-carboxamide (5b). From **20a** [33] and using aniline as reagent. Yield 36%, mp = 227-230 °C (EtOH). ^{1}H NMR (400 MHz, DMSO-d_6) δ 12.16 (exch br s, 1H, NH), 9.29 (s, 1H, Ar), 8.62 (d, 1H, *J* = 8.1 Hz, Ar),

7.72 (d, 2H, *J* = 8.0 Hz, Ar), 7.53 (d, 1H, *J* = 8.1 Hz, Ar), 7.46-7.35 (m, 6H, Ar), 7.13-7.09 (m, 1H, Ar), 5.83 (s, 2H, CH_2), 2.65 (s, 3H, CH_3). ^{13}C NMR (100 MHz, DMSO-*d*$_6$) δ 176.23 (C), 163.54 (C), 161.89 (C), 148.81 (CH), 148.24 (C), 138.53 (C), 136.05 (CH), 135.67 (C), 132.49 (C), 129.87 (2×CH), 129.05 (2×CH), 128.62 (2×CH), 123.64 (CH), 122.00 (CH), 119.65 (2×CH), 119.52 (C), 112.18 (C), 52.33 (CH_2), 24.74 (CH_3). HR-MS(ESI): calcd for $C_{22}H_{18}ClN_3O_2$ 403.1088 (m/z), found m/z 404.1170, 406.1150 $[M + H]^+$, m/z 426.0990, 428.0969 $[M + Na]^+$. t_R= 36.073 min.

N-6-Dimethyl-4-oxo-N-phenyl-4H-pyrido[1,2-a]pyrimidine-3-carboxamide (5d). From **21** [33] and using N-methylaniline as reagent. Yield 45%, mp = 193-195 °C (EtOH). ^{1}H NMR (400 MHz, DMSO-*d*$_6$) δ 8.27 (s, 1H, Ar), 7.72-7.68 (m, 1H, Ar), 7.39 (d, 1H, *J* = 8.0 Hz, Ar), 7.25-7.14 (m, 5H, Ph), 6.94 (d, 1H, *J* = 4.0 Hz, Ar), 3.35 (s, 3H, CH_3), 2.44 (s, 3H, CH_3). ^{13}C NMR (100 MHz, DMSO-*d*$_6$) δ 165.32 (C), 157.02 (C), 153.58 (C), 153.28 (CH), 143.74 (C), 143.24 (C), 137.28 (CH), 128.39 (2×CH), 126.64 (2×CH), 126.54 (CH), 124.50 (CH), 119.49 (CH), 115.50 (C), 36.89 (CH_3), 22.77 (CH_3). HR-MS(ESI): calcd for $C_{17}H_{15}N_3O_2$ 293.1164 (m/z), found m/z 294.1253 $[M + H]^+$, m/z 316.1092 $[M + Na]^+$. t_R= 22.837 min.

N-(3,5-Dichloropyridin-4-yl)-7-methyl-4-oxo-1-phenyl-1,4-dihydro-1,8-naphthyridine-3-carboxamide (5c). NaH (0.43 mmol) was added to a cooled (0 °C) solution of 3,5-dichloro-4-pyridilamine (0.43 mmol) in anhydrous THF (3 mL), and the mixture was stirred for 3 h. The acyl chloride (0.43 mmol), obtained using $SOCl_2$ and triethylamine following the same procedure reported for **5b** and **5d**, in anhydrous THF (3 mL) was then added to the mixture at 0 °C. After 30 min, the solvent was removed, and the residue was sequentially washed with 6 M NaOH (2 × 10 mL), 2N HCl (2 × 10 mL) and H_2O. The solid residue was purified by flash column chromatography using cyclohexane/ethyl acetate 2:1 as eluent. From **20b** [33], yield 60%, mp = 229-230 °C (EtOH). ^{1}H NMR (400 MHz, DMSO-*d*$_6$) δ 12.12 (exch br s, 1H, NH), 8.79 (s, 1H, Ar), 8.72-8.68 (m, 3H, Ar), 7.66-7.55 (m, 6H, Ar), 2.51 (s, 3H, CH_3). ^{13}C NMR (100 MHz, DMSO-*d*$_6$) δ 176.61 (C), 163.74 (C), 161.17 (C), 149.53 (C), 149.14 (CH), 148.08 (2×CH), 140.54 (C), 140.43 (C), 135.81 (CH), 129.26 (2×CH), 129.20 (CH), 129.17 (2×C), 127.65 (2×CH), 122.34 (CH), 119.22 (C), 110.73 (C), 24.78

(CH_3). HR-MS(ESI): calcd for $C_{21}H_{14}Cl_2N_4O_2$ 424.0494 (m/z), found m/z 425.0571, 427.0545 [M + Na]$^+$, 447.0394, 449.0368 [M + Na]$^+$. t_R= 31.830 min.

5,6-Dimethyl-2-phenylpyrazolo[1,5-a]pyrimidin-7(4H)-one (7). A solution of commercially available **6** (1.0 mmol) and ethyl-2-methyl-3-oxobutanoate (1.0 mmol) in ethanol, containing a catalytic amount of acetic acid, was refluxed for 10-30 minutes. After cooling, the precipitate was filtered off and washed with ethanol/water and recrystallized from ethanol. Yield 72 %, mp > 300 °C; ^{1}H NMR (400 MHz, DMSO-d_6) δ 8.01 (d, 1H, J = 7.9 Hz, Ar), 7.47 (t, 1H, J = 7.3 Hz, Ar), 7.53-7.34 (m, 3H, Ar), 6.17 (s, 1H, Ar), 1.88 (s, 3H, CH_3), 2.35 (s, 3H, CH_3).

3-Amino-5-methyl-2-phenylpyrazolo[1,5-a]pyrimidin-7(4H)-one (11)

A catalytic amount of Pd/C was added to compound **10** [35] (4.0 mmol) suspended in ethanol (150 mL). The reduction (hydrogen in a Parr equipment) was complete in 2 hours. The suspension was then filtered off to remove the catalyst and the solution obtained was evaporated under vacuum. The yellow crude product was of suitable purity to be directly used in the next reaction. Yield 57%, mp > 300 °C; ^{1}H-NMR (400 MHz, DMSO-d_6) δ 7.57 (dd, 1H, J = 7.8, 1.5 Hz, Ar), 7.45 (exch br s, 1H, NH), 7.64-7.38 (m, 5H, J = 7.8 Hz Ar), 5.40 (exch br s, 2H, NH_2), 2.39 (s, 3H, CH_3).

5-Amino-3-(3-chlorophenyl)-1-(cyclopentylmethyl)-6-oxo-1,6-dihydropyridazine-4-carboxamide (17b). A mixture of the 5-amino-1,6-dihydropyridazine-4-carboxylic acid amide **16b** [33] (0.49 mmol), K_2CO_3 (0.98 mmol) and 1.23 mmol of (bromomethyl)cyclopentane was stirred in anhydrous DMF (1 mL) at 80 °C for 2 h. After cooling, ice-cold water was added and the precipitate was recovered by filtration under vacuum to give the pure intermediate **17b**. Yield 59%, mp = 184-187 °C (EtOH). ^{1}H NMR (400 MHz, $CDCl_3$) δ 7.55 (s, 1H, Ar), 7.50-7.37 (m, 3H, Ar), 5.39 (exch br s, 1H, $CONH_2$), 4.95 (exch br s, 1H, $CONH_2$), 4.16 (s, 2H, -*CH_2*-cC_5H_9), 2.54 (m, 1H, CH cC_5H_9), 1.80-1.60 (m, 5H, cC_5H_9), 1.42-1.23 (m, 3H, cC_5H_9).

4.3. Pharmacology

4.3.1. Cell Culture

NanoLuc (Nluc) A_1R or A_3R expressing human embryonic kidney (HEK293) cells were cultured in Dulbucco's Modified Eagle Medium (DMEM)/Nutrient mixture F12 supplemented with 10% heat-inactivated foetal bovine serum (FBS) and 1% antibiotic-antimycotic (AA) solution, in the presence of 800µg/mL G418. Chinese Hamster Ovary (CHO) K1 cells stably expressing A_1R, $A_{2a}R$, $A_{2b}R$, or A_3R were cultured in Nutrient mixture F12 supplemented with 10% FBS and 1% AA, in the presence of 600µg/mL G418. Flp-In™-CHO cells expressing the rat A_3R were cultured in Nutrient mixture F12 supplemented with 10% FBS and 1% AA, in the presence of 600µg/mL Hygromycin-B. Cells were cultured at 37°C in a humidified incubator with 5% CO_2.

4.3.2. NanoBRET Ligand Binding Assay

Ligand binding assays were performed as previously described [37,38]. Cells were treated with CA200645 at 15nM for Nluc-A_3R and 40nM for A_1R, and unlabelled test compounds in the concentration range 100µM to 1nM. 10nM MRS1220 or 100nM DPCPX was used to determine non-specific binding.

4.3.3. cAMP Accumulation Assays

Measurement of cAMP accumulation was performed as previously described [37,38], using the LANCE*ultra* cAMP detection kit. CHO-K1 cells stably expressing A_1R, A_3R, $A_{2a}R$, or $A_{2b}R$, or Flp-In™-CHO cells expressing the rat A_3R were seeded at 1000 cells per well of a 384-well OptiPlate. Cells were stimulated with NECA in the concentration range 100 µM to 0.1 nM (1 µM to 1 pM for A_1R and 10 µM to 10 pM for rat A_3R) in the absence or presence of test compounds (with the addition of forskolin at 1 or 10 µM for A_3R and A_1R respectively) for 30-minutes. Data were normalised to the response to 100 µM forskolin or in the case of the rat A_3R, the range of NECA in the absence of test compounds.

4.3.4. Data Analysis

Data was analysed using GraphPad Prism 10. pKi values were determined using the "One site – fit Ki" model, and pEC50 values determined using the "log(agonist) vs. response (three parameters)" equation. pKb values were calculated using the Schild Equation:

$$K_b = \frac{X_b}{DR - 1}$$

Where X_b is the antagonist concentration, and DR the dose ratio, defined by:

$$DR = \frac{EC_{50(with\ antagonist)}}{EC_{50(agonist\ alone)}}$$

4.4. Molecular Docking

The structures of the active and inactive state A_1R were obtained from the RCSB Protein Data Bank. The inactive form used was the crystal structure of A_1R receptor bound to antagonist, PSB36 (PDB: 5N2S), where the antagonist was removed before performing the docking [44]. The active form was the cryo-EM structure of the A_1R bound to adenosine in complex with G*ai2* (PDB: 6D9H) [45]. Both adenosine and G*ai2* protein were removed before performing the docking. The inactive form of the A_3R was obtained from Stampelou *et al* [46]. The active structure used was the cryo-EM structure of A_3R bound to CF101 (PDB: 8X16), with the selective agonist removed before performing the docking [47].

Heteroatoms were removed from the protein before the protein preparation and processing. Hydrogens were added and the protonation state was set at the physiological pH of 7.4. Kollman charges were assigned to the protein during PDBQT conversion. For ligand preparation, the Avogadro molecular editor was used to generate the 3D structure file [48]. Hydrogens were added and Gasteiger charges were calculated for each ligand. An affinity grid of 30x30x30 Å with 0.375 Å spacing centered on the respective binding sites were generated using Autogrid. This allowed for a comprehensive grid box to be generated to incorporate all potential docking poses within the orthosteric pocket observed in the structures. Ligand docking was performed using AutoDock Vina

[49,50]. The electrostatic surface potentials for the protein was generated through the APBS-PDB2PQR software suite [42]. These resources are available from the APBS/PDB2PQR server, https://server.poissonboltzmann.org/ (accessed 12 July 2024). PQR files were generated at a pH of 7.4 using the AMBER forcefield and were visualized through the APBS-Pymol 3.0 plugin. Ligand interaction diagrams were generated through Ligplot+ v2.2 [51].

CRediT authorship contribution statement

Letizia Crocetti: Writing – original draft, Conceptualization, Supervision, Writing – review & editing, Project administration. **Abigail Pearce:** Methodology, Data curation, Formal analysis, Writing – review & editing. **Venkat S. Vege:** Data curation, Software, Methodology, Writing – review & editing. **Qi Xu:** Methodology, Data curation, Formal analysis, Writing – original draft, Validation. **Jing Xu:** Methodology, Data curation, Formal analysis. **Maria Paola Giovannoni:** Conceptualization, Writing – review & editing. **Gabriella Guerrini:** Writing – original draft, Validation. **Francesca Catarzi:** Formal analysis, Methodology. **Hannes Buthmann**: Data Curation, Visualization, Methodology. **Xianglin Huang:** Data Curation, Methodology. **Aneesh Chandran:** Validation, Writing – review & editing. **Graham Ladds:** Writing – review & editing, Supervision, Funding acquisition, Conceptualization, Project administration. **Agostino Cilibrizzi:** Writing – review & editing, Supervision, Funding acquisition, Project administration, Conceptualization. All the authors have given approval to the final version of the manuscript.

Declaration of competing interest

The authors declare that they have no known competing financial interests or personal relationships that could have appeared to influence the work reported in this paper.

Acknowledgements

Q.X. (KCL) and X.H (Cambridge) are funded by China Scholarship Council International Scholarships. Work in G.L.'s lab is funded by the BBSRC (BB/Y513817/1, to A.C; BB/W014831/1, A.P.). We thank the David James Trust fund for funding V.S.V. G.L. is a Royal Society Industry Fellow (INF/R2/212001).

References

[1] B.B. Fredholm, A.P. IJzerman, K.A. Jacobson, K.N Klotz, J. Linden, International Union of Pharmacology. XXV. Nomenclature and classification of adenosine receptors, Pharmacol. Rev. 53(4) (2001) 527-52.

[2] A.P. IJzerman, K.A. Jacobson, C.E. Muller, B.N. Cronstein, R.A. Cunha, International union of basic and clinical pharmacology. CXII: adenosine receptors: a further update, Pharmacol. Rev. 74 (2022) 340-372.

[3] S. Moro, Z.G. Gao, K.A. Jacobson, G. Spalluto, Progress in the pursuit of therapeutic adenosine receptor antagonists, Med. Res. Rev. 26(2) (2006) 131-159.

[4] A.S. Hauser, M. M. Attwood, M. Rask-Andersen, H.B. Schiöth, D.E. Gloriam, Trends in GPCR drug discovery: New agents, targets and indications, Nat. Rev. Drug Discov. 16 (2017) 829-842.

[5] V. Vallon, H. Osswald, Adenosine receptors and the kidney, adenosine aeceptors in health and disease, Handb. Exp. Pharmacol. 193 (2009) 443-470.

[6] M.R. Blackburn, C.O. Vance, E. Morschl, C.N. Wilson, Adenosine receptors and inflammation, Adenosine receptors in health and disease, Handb. Exp. Pharmacol. 193 (2009) 215-269.

[7] J.C. Shryock, L. Belardinelli, Adenosine and adenosine receptors in the cardiovascular system: biochemistry, physiology, and pharmacology, Am. J. Cardiol. 79(12A) (1997) 2-10.

[8] S.S. Gottlieb, S.L. Skettino, A. Wolff, E. Beckman, M.L. Fisher, R. Freudenberger, T. Gladwell, J. Marshall, M. Cines, D. Bennett, E.B. Liittschwager, Effects of BG9719 (CVT-

124), an A1-adenosine receptor antagonist, and furosemide on glomerular filtration rate and natriuresis in patients with congestive heart failure, J. Am. Coll. Cardiol. 35(1) (2000) 56-59.

[9] C. Falcone, M. Caracciolo, P. Correale, S. Macheda, E.G. Vadalà, S. La Scala, M. Tescione, R. Danieli, A. Ferrarelli, M.G. Tarsitano, L. Romano, A. De Lorenzo, Can adenosine fight COVID-19 acute respiratory distress syndrome? J. Clin. Med. 9 (2020) 3045.

[10] P. Correale, M. Caracciolo, F. Bilotta, M. Conte, M. Cuzzola, C. Falcone, A.C. Falzea, E. Iuliano, A. Morabito, G. Foti, A. Armentano, M. Caraglia, A. De Lorenzo, M. Sitkovsky, S. Macheda, Therapeutic effects of adenosine in high flow 21% oxygen aerosol in patients with Covid19-pneumonia, PLoS one 15 (2020) e0239692.

[11] J.A. Ribeiro, A.M. Sebastião, A. de Mendonça, Adenosine receptors in the nervous system: pathophysiological implications, Prog. Neurobiol. 68(6) (2002) 377-392.

[12] J.L. Albasanz, S. Perez, M. Barrachina, I. Ferrer, M. Martín, Up-regulation of adenosine regulation of adenosine receptors in the frontal cortex in Alzheimer's disease, Brain Pathol. 18(2) (2008) 211-219.

[13] K.A. Jacobson, P.J.M. Van Galen, M. Williams, Adenosine receptors: pharmacology, structure-activity relationships, and therapeutic potential, J. Med. Chem. 35(3) (1992) 407-422.

[14] T. Maemoto, M. Tada, T. Mihara, N. Ueyama, H. Matsuoka, K. Harada, T. Yamaji, K. Shirakawa, S. Kuroda, A. Akahane, A. Iwashita, N. Matsuoka, S. Mutoh, Pharmacological characterization of FR194921, a new potent, selective, and orally active antagonist for characterization of central adenosine A1 receptors, J. Pharmacol. Sci. 96(1) (2004) 42-52.

[15] P.N.H. Trinh, J.A. Baltos, S.D. Hellyer, L.T. May, K.J. Gregory, Adenosine receptor signalling in Alzheimer's disease, Purinergic. Signal. 18(3) (2022) 359-381.

[16] J.P. Lopes, A. Pliassova, R.A. Cunha, The physiological effects of caffeine on synaptic transmission and plasticity in the mouse hippocampus selectively depend on adenosine A_1 and A_{2A} receptors, Biochem. Pharmacol. 166 (2019) 313-321.

[17] C.L. Zuo, C.M. Wang, J. Liu, T. Shen, J.P. Zhou, X.R. Hao, Y.Z Pan, H.C. Liu, Q.Q. Lian, H. Lin, Isoflurane anesthesia in aged mice and effects of A1 adenosine receptors on cognitive impairment, CNS Neurosci. Ther. 24(3) (2018) 212-221.

[18] S. Merighi, M. Nigro, A. Travagli, S. Pasquini, P.A. Borea, K. Varani, F. Vincenzi, S. Gessi, A_{2A} Adenosine receptor: a possible therapeutic target for Alzheimer's disease by regulating NLRP3 inflammasome activity? Int. J. Mol. Sci. 23(9) (2022) 5056.

[19] Z.G. Gao, J.A. Auchampach, K.A. Jacobson, Species dependences of A_3 adenosine receptor pharmacology, Purinergic. Signal. 19 (2023) 523-550.

[20] E. Coppi, F. Cherchi, M. Venturini, E. Lucarini, R. Corradetti, L. Di Cesare Mannelli, C. Ghelardini, F. Pedata, A.M. Pugliese, Therapeutic potential of highly selective A_3 adenosine receptor ligands in the central and peripheral nervous system, Molecules 27 (2022) 1890.

[21] F. Vincenzi, S. Pasquini, C. Contri, M. Cappello, M. Nigro, A. Travagli, S. Merighi, S. Gessi, P.A. Borea, K. Varani, Pharmacology of adenosine receptors: recent advancements, Biomolecules 13 (2023) 1387.

[22] C. Mazziotta, J.C. Rotondo, C. Lanzillotti, G. Campione, F. Martini, M. Tognon, Cancer biology and molecular genetics of A_3 adenosine receptor. Oncogene 41 (2022) 301-308.

[23] J. Wang, A. Bhattarai, H. N Do, S. Akhter, Y.L. Miao, Molecular simulations and drug discovery of adenosine receptors, Molecules 27 (2022) 2054.

[24] A. Glukhova, D.M. Thal, A.T. Nguyen, E.A. Vecchio, M. Jörg, P.J. Scammells, L.T. May1, P.M. Sexton, Structure of the adenosine A_1 receptor reveals the basis for subtype selectivity, Cell. 168(5) (2017) 867-877.

[25] K.A. Jacobson and Z.G. Gao, Adenosine receptors as therapeutic targets, Nat. Rev. Drug Discov. 5(3) (2006) 247-264.

[26] M.P. Giovannoni, G. Ciciani, A. Cilibrizzi, L. Crocetti, S. Daniele, L. Di Cesare Mannelli, C. Ghelardini, C. Giacomelli, G. Guerrini, C. Martini, M.L. Trincavelli, C. Vergelli, Further

studies on pyrazolo[1',5':1,6]pyrimido[4,5-d]pyridazin-4(3H)-ones as potent and selective human A_1 adenosine receptor antagonists, Eur. J. Med. Chem. 89 (2015) 32-41.

[27] A. Graziano, M.P. Giovannoni, A. Cilibrizzi, L. Crocetti, V. Dal Piaz, C. Vergelli, M.L. Trincavelli, C. Martini, C. Giacomelli, New pyrazolo[1',5':1,6]pyrimido[4,5-d]pyridazin-4(3H)-ones fluoroderivatives as human A_1 adenosine receptor ligands, Acta Chim. Slov. 59(3) (2012) 648-655.

[28] M.P. Giovannoni, C. Vergelli, A. Cilibrizzi, L. Crocetti, C. Biancalani, A. Graziano, V. Dal Piaz, M.I. Loza, M.I. Cadavid, J.L. Díaz, A. Gavaldà, Pyrazolo[1′,5′:1,6]pyrimido[4,5-d]pyridazin-4(3H)-ones as selective human A_1 adenosine receptor ligands, Bioorg. Med. Chem. 18 (22) (2010) 7890-7899.

[29] L. Vettori Pecori, L. Cecchi, A. Costanzo, G. Auzzi, F. Bruni, New pharmacologically active 2-phenylpyrazolo[1,5-a]pyrimidines, Farmaco, Edizione Scientifica 36(6) (1981) 441-448.

[30] G. Auzzi, L. Cecchi, A. Costanzo, L. Pecori Vettori, F. Bruni, Structure of pyrazolo[1,5-a]pyrimidine methylderivatives, Farmaco, Edizione Scientifica 33(1) (1978) 14-20.

[31] M. Ridi, P. Papini, and S. Cecchi, Investigations in the seriesof pyrazolo[2,3-a]pyrimidine and pyrazolo[3,4-b]pyridine, Gazzetta Chimica Italiana 91 (1961) 973-986.

[32] L. Pecori Vettori, G. Auzzi, F. Bruni, A. Costanzo, Synthesis of some 7-phenylpyrrolo[1,2-a]pyrimidine derivatives. III, Farmaco, Edizione Scientifica 42(11) (1987) 787-792.

[33] L. Crocetti, G. Floresta, S. Nazir, C. Vergelli, A. Bhogal, C. Biancalani, N. Cesari, M.P. Giovannoni, A. Cilibrizzi, Synthesis and inverse virtual screening of new bi-cyclic structures towards cancer-relevant cellular targets, Struct. Chem. 33 (2022) 769-793.

[34] S. Checchi, M. Ridi, P. Papini, 5-Aminopyrazole derivatives. II. The reactivity of 3-phenyl-5-aminopyrazole and some of its derivatives, Gazzetta Chimica Italiana 85 (1955) 1558-1569.

[35] S. Checchi, P. Papini, M. Ridi, 5-Aminopyrazole derivatives. III. The reactivity of 3-phenyl-5-aminopyrazole and some of its derivatives, Gazzetta Chimica Italiana 85 (1955) 1160-1170.

[36] G.M. Abdalla,J.W. Sowell, Synthesis of 8-cyano-1,4-dihydro-4-oxopyrrolo[1,2-a]pyrimidine-3-carboxylic acids as potential antimicrobial agents, J. Heterocycl. Chem. 24(2) (1987) 297-301.

[37] K. Barkan, P. Lagarias, M. Stampelou, D. Stamatis, S. Hoare, D. Safitri, K.N. Klotz, E. Vrontaki, A. Kolocouris, G. Ladds, Pharmacological characterisation of novel adenosine A_3 receptor antagonists, Sci. Rep. 10(1) (2020) 20781.

[38] M. Stampelou, A. Suchankova, E. Tzortzini, L. Dhingra, K. Barkan, N. Lougiakis, P. Marakos, N. Pouli, G. Ladds, A. Kolocouris, Dual A1/A3 adenosine receptor antagonists: binding kinetics and structure-activity relationship studies using mutagenesis and alchemical binding free energy calculations, J. Med. Chem. 65 (2022) 13305-13327.

[39] R.J. Tallarida, R.B. Murray, Manual of pharmacologic calculations with computer programs, Springer New York, NY (1987).

[40] M. Lu, B. Wang, C. Zhang, X. Zhuang, M. Yuan, H. Wang, W. Li, R. Su, J. Li, PQ-69, a novel and selective adenosine A_1 receptor antagonist with inverse agonist activity, Purinergic. Signal. 10(4) (2014) 619-629.

[41] J.A. Ballesteros, H. Weinstein, Integrated methods for the construction of three-dimensional models and computational probing of structure-function relations in G protein-coupled receptors, Neurosci. Methods 25 (1995) 366-428.

[42] C. de Graaf, N. Foata, O. Engkvist, D. Rognan, Molecular modeling of the second intracellular loop of G-protein coupled receptors and its implication on structure-based virtual screening, Proteins, 71(2) (2008) 599-620.

[43] E. Jurrus, D. Engel, K. Star, K. Monson, J. Brandi, L.E. Felberg, D.H. Brookes, L. Wilson, J. Chen, K. Liles, M. Chun, P. Li, D.W. Gohara, T. Dolinsky, R. Konecny, D.R. Koes, J.E. Nielsen, T. Head-Gordon, W. Geng, R. Krasny, G.W. Wei, M.J. Holst, J.A. McCammon, N.A. Baker, Improvements to the APBS biomolecular solvation software suite, Protein Sci. 27(1) (2018) 112-128.

[44] R.K.Y. Cheng, E. Segala, N. Robertson, F.H. Marshall, R.M. Cooke, J.C. Errey, F.H. Marshall, R.M. Cooke, Structures of human A1 and A_{2A} adenosine receptors with xanthines reveal determinants of article structures of human A1 and A_{2A} adenosine receptors with xanthines reveal determinants of selectivity, Structure 25 (2017) 1275-1285.

[45] C. J. Draper-Joyce, M. Khoshouei, D.M. Thal, Y.L. Liang, A.T.N. Nguyen, S.G.B. Furness, H. Venugopal, J.A. Baltos, J.M. Plitzko, R. Danev, W. Baumeister, L.T. May, D. Wootten, P.M. Sexton, A. Glukhova, A. Christopoulos, Structure of the adenosine-bound human adenosine A_1 receptor–Gi complex, Nature 558 (7711) (2018) 559-563.

[46] M. Stampelou, G. Ladds, A. Kolocouris, Computational workflow for refining AlphaFold models in drug design using kinetic and thermodynamic binding calculations: a case study for the unresolved inactive human adenosine A3 receptor, J. Phys. Chem. B 128 (2024) 914- 936.

[47] H. Cai, S. Guo, Y. Xu, J. Sun, J. Li, Z. Xia, Y. Jiang, X. Xie, H. Xu, Cryo-EM structures of adenosine receptor A_3AR bound to selective agonists, Nat. Commun. 15 (2024) 3252.

[48] M.D. Hanwell, D.E. Curtis, D.C Lonie, T. Vandermeersch, E. Zurek, G.R. Hutchison, "Avogadro: an advanced semantic chemical editor, visualization, and analysis platform", J. ChemInf. 4 (2012) 17.

[49] J. Eberhardt, D. Santos-Martins, A. F. Tillack, S. Forli, AutoDock Vina 1.2.0: New docking methods, expanded force field, and python bindings, J. Chem. Inf. Model. 61 (2021) 3891-3898.

[50] O. Trott, A.J. Olson, AutoDock Vina: improving the speed and accuracy of docking with a new scoring function, efficient optimization and multithreading, J. Comput. Chem. 31 (2010) 455-461.

[51] R.A. Laskowski and M.B. Swindells, LigPlot+: multiple ligand-protein interaction diagrams for drug discovery, J. Chem. Inf. Model. 51 (2011) 2778-2786.